A Two-Stage Strategy for Retrieving 2-D Ocean Wave Spectra From Chinese Gaofen-3 SAR Wave Mode Products

Yuxin Fang, Chenqing Fan, Rui Cao, Junmin Meng, Jie Zhang, and Qiushuang Yan

***Abstract*—Synthetic aperture radar (SAR) is widely used for observing sea surfaces and retrieving 2-D wave spectra. However, existing methods for retrieving directional wave spectra from SAR imagettes face challenges due to the complex nonlinear SAR-wave imaging relationship and the limitation of first-guess spectra. This study proposes a novel two-stage machine learning strategy for retrieving 2-D directional wave spectra from Chinese Gaofen-3 SAR wave mode products. We achieve the generation of complete 2-D wave spectra and several wave parameters solely from GF-3 SAR data without necessitating any additional inputs. In the first stage, we employ the Energy Attention Conditional Generative Adversarial Network (EA-CGAN) to retrieve the normalized wave spectrum. The generator of the EA-CGAN establishes a nonlinear transformation from normalized SAR cross spectra to normalized wave spectra to enhance the capabilities. In the second stage, the XGBoost model retrieves the intensity of the wave spectrum. The EA-CGAN and XGBoost models were trained on an extensive dataset that consists of about 11 000 Gaofen-3 SAR wave mode imagettes and 2-D wave spectra from the fifth-generation reanalysis (ERA-5) of the European Centre for Medium-Range Weather Forecasts. The results of the evaluation using test samples reveal high consistency between the retrieved wave spectra and ERA-5 wave spectra in terms of spectral similarity, peak period, peak direction, significant wave height, and mean wave periods. Compared to the traditional methods, our approach offers enhanced effectiveness, demonstrating the potential of advanced deep learning in high-precision SAR wave spectrum inversion.**

Manuscript received 2 February 2024; revised 1 April 2024; accepted 24 April 2024. Date of publication 26 April 2024; date of current version 30 May 2024. This work was supported in part by the National Natural Science Foundation of China (NSFC) under Grant 61931025 and Grant 42206178, in part by the Natural Science Foundation of Shandong Province under Grant ZR2021QD010, in part by the Fund of Technology Innovation Center for Ocean Telemetry, Ministry of Natural Resources under Grant 2022003, in part by the Innovation fund project for graduate student of China University of Petroleum (East China) under Grant 23CX04006A, and in part by the Fundamental Research Funds for the Central Universities. *(Corresponding author: Qiushuang Yan.)*

Yuxin Fang is with the College of Oceanography and Space Informatics, China University of Petroleum (East China), Qingdao 266580, China, and also with the Department of Civil and Environmental Engineering, Imperial College London, SW7 2AZ London, U.K. (e-mail: fangyuxin_upc@163.com).

Chenqing Fan and Junmin Meng are with the First Institute of Oceanography, Ministry of Natural Resources, Qingdao 266061, China.

Rui Cao is with the Department of Civil and Environmental Engineering, Imperial College London, SW7 2AZ London, U.K. (e-mail: rui.cao17@imperial.ac.uk).

Jie Zhang is with the First Institute of Oceanography, Ministry of Natural Resources, Qingdao 266061, China, and also with the College of Oceanography and Space Informatics, China University of Petroleum (East China), Qingdao 266580, China (e-mail: zhangjie@fio.org.cn).

Qiushuang Yan is with the College of Oceanography and Space Informatics, China University of Petroleum (East China), Qingdao 266580, China (e-mail: yanqiushuang@upc.edu.cn).

Digital Object Identifier 10.1109/JSTARS.2024.3394057

***Index Terms*—Gaofen-3, generative adversarial net, ocean wave parameters, synthetic aperture radar (SAR), 2-D wave spectrum.**

I. Introduction

THE 2-D wave spectrum serves as a powerful tool for statistically characterizing the entirety of ocean waves, providing a comprehensive description of the distribution of wave energy. From the 2-D wave spectrum, one can extract various statistical features that encapsulate the nature of the waves, including significant wave height, average wave period, and the characteristic wavelength. This analytical approach holds significant importance in the realm of marine meteorology, navigation, and offshore, and coastal activities [1]. The precision with which we observe and interpret 2-D wave spectra is pivotal for advancing our understanding and enhancing the reliability of predictions in these crucial domains.

The precise global measurement of 2-D wave spectra, however, still poses a significant challenge. Currently, information on wave spectra is primarily obtained through two main methods: 1) wave buoys; and 2) satellite remote sensing. Wave buoys stand out as one of the most authoritative means to acquire wave spectra and corresponding integrated wave variables. Nevertheless, their effectiveness is constrained by the limited spatial distribution of these buoys because they only provide point measurements. In contrast, spaceborne synthetic aperture radar (SAR) has become as a powerful tool for detecting the sea state evolution over expansive areas with high spatial resolution, operating effectively under different weather conditions [2], [3], [4]. However, the retrieval of wave spectra from SAR data is intricate due to the nonauthentic nature of SAR imagettes of the sea surface. Numerous attempts have been made to develop theoretical algorithms for wave spectrum retrieval from SAR imagettes [5], [6], [7], [8], [9].

Recent advancements in satellite technology and the release of massive datasets have motivated research focusing on the extraction of individual ocean wave parameters from SAR features using empirical algorithms. The subsequent sections (i.e., Sections I-A and I-B) aim to provide a comprehensive review of both theoretical and empirical research in this field.

A. Review of Theoretical Wave Spectrum Retrieval Methods

1) Motivation: A nonlinear imaging mechanism exists between the SAR imagettes and ocean waves, which forms the

© 2024 The Authors. This work is licensed under a Creative Commons Attribution-NonCommercial-NoDerivatives 4.0 License. For more information, see https://creativecommons.org/licenses/by-nc-nd/4.0/

foundation for theoretical wave spectrum retrieval methods by establishing a nonlinear integral transformation between wave spectra and SAR spectra. In essence, the total nonlinear transformation includes tilt and hydrodynamic modulation functions, along with nonlinear velocity bunching [10]. The goal is therefore to retrieve the anticipated wave spectra by minimizing the cost function associated with the nonlinear transformation.

2) Literature Review: One of the pioneering nonlinear wave spectral retrieval methods is the Max Planck Institute (MPI) approach proposed by Hasselmann and Hasselmann [2]. This method establishes a nonlinear mapping relationship, necessitating a first-guess wave spectrum to reconstruct the complete retrieval spectrum. Building upon the MPI method, Krogstad [3] provided a simplified derivation of the nonlinear transformation. Hasselmann et al. [4] further enhanced the MPI method by refining the cost function and introducing an additional iteration. These MPI-based retrieval techniques have been instrumental in generating global ERS-1 SAR wave mode data, utilizing numerical wave models and demonstrating promising results [5], [11]. In addition, Mastenbroek et al. [12] introduced a semiparametric algorithm (SPRA) that incorporates wind scatterometer data as supplementary inputs. In a distinct approach, Sun and Guan [13] developed the Parameterized First-guess Spectrum Method (PFSM) to separately retrieve the wind-sea component and the linear-mapping swell. Unlike MPI-based methods, Engen and Johnsen [14] utilized SAR cross spectra for wave spectrum inversion. The SAR cross spectra, derived from individual look SAR imagettes, not only provide information on wave propagation direction, but also effectively reduce speckle noise. These cross-spectrum-based methods have been successfully applied in ENVISAT ASAR wave mode Level-2 products [15]. Further advancements include the Partition Rescaling and Shift Algorithm (PARSA) [16], which combines numerical WAM information with SAR cross spectra to achieve promising retrieval results. Although this method can reduce the cutoff effects, it requires prior information so it is inconvenient in practical applications.

3) Limitations: Despite their significant contributions, there are some limitations on the wave spectrum retrieval methods of MPI, SPRA, PFSM, and PARSA. These approaches need prior information, such as a first-guess wave spectrum or wind vectors, posing challenges in practical applications where obtaining such information may be inconvenient. Moreover, the presence of conflicting propagating wave factors within the first-guess wave spectrum can result in errors in standard wave retrieval. The performance of cross-spectrum-based wave spectrum retrieval methods is in large part constrained by the cutoff wavenumber, as they lack additional input information about ocean waves. Specifically, the distortion in SAR imaging mechanisms caused by the Doppler frequency shift erases information about waves propagating in the azimuth direction of SAR. Besides, while the retrieved swell information is generally acceptable, the representation of wind wave information remains incomplete. At present, the modulation transfer functions governing the nonlinear relationship are not well understood [9], which decreases the effectiveness of establishing this nonlinear relationship. The hydrodynamic contribution, linked to weak polarization dependence according to theoretical studies and tower measurements [17], adds to the complexity of the nonlinear transformation. In addition, the iterative updating process required for retrieval wave spectra is time-consuming, hindering the feasibility of these methods for commercial applications.

B. Review of Empirical Wave Parameter Retrieval

1) Motivation: Empirical algorithms offer an alternative approach to wave parameter retrieval, bypassing the complexities associated with establishing nonlinear mappings. Instead, these algorithms directly invert multiple wave parameters from SAR features. Over the past decade, numerous empirical models have been proposed, leveraging the wealth of available SAR ocean scenes.

2) Literature Review: The classical empirical algorithms are a series of CWAVE models [18], [19], [20]. These models retrieve significant wave height by utilizing two SAR imagettes-based variables (i.e., the normalized radar cross section (NRCS) and the normalized imagettes variance (cvar)) and 20 spectral parameters calculated from the normalized SAR imagettes spectrum. A variety of semiempirical and empirical models [21], [22], [23], [24], [25], [26], [27] have been proposed to retrieve significant wave height from variables such as azimuth cutoff wavelength (λ_c), peak wavelength (λ_p), peak wave direction (ϕ), NRCS, cvar, NRCS skewness (skew), NRCS kurtosis (kurt), and incidence angle (θ). Collins et al. [28] explored the effects of different SAR polarizations, while Pramudya et al. [25] focused on enhancing empirical SAR significant wave height estimation by combining multiple polarizations. In terms of machine learning, various approaches [29], [30] have been proposed to predict significant wave height using single- or multipolarization SAR features. With the evolution of deep learning in image processing, models based on deep learning have emerged as effective tools for retrieving wave parameters from SAR features. It should be noted recent advancements consider 2-D image-level features containing energy distribution information for significant wave height retrieval [31], [32].

3) Limitations: The primary limitation of the empirical methods is that they focus only on retrieving one specific ocean wave parameter, lacking the capability to invert the complete 2-D ocean wave spectrum. The 2-D frequency direction wave spectrum, which is capable of providing a more accurate and thorough depiction of waves, remains beyond the reach of these empirical approaches. Consequently, there is an urgent need to develop intelligent retrieval technologies that can effectively retrieve 2-D ocean wave spectra from SAR products.

C. Our Two-Stage Retrieval Strategy for Retrieving 2-D Wave Spectra From SAR Products

The objective in this study is to retrieve complete 2-D wave spectra only from the provided SAR products, without the need for prior information inputs. This then enables the simultaneous extraction of various sea state elements, including significant wave height, average wave period, and peak wave direction. To achieve this, we introduce a two-stage retrieval strategy,

consisting of the retrieval of wave spectrum energy distribution and wave spectrum energy intensity.

Based on a Gaofen-3 SAR wave mode product, the first stage (termed wave spectrum energy distribution retrieval) is to output the normalized wave spectrum $S_{0-1}(k_x, k_y)$, which effectively captures the distribution of wave energy. This strategy employs a direct transform model that establishes a relationship between normalized SAR cross-spectra and normalized wave spectra through data-driven approaches. By doing so, we circumvent the challenges associated with a highly complex and constrained nonlinear transformation, especially considering the limited understanding of hydrodynamic modulation. The transform model takes a normalized SAR cross-spectrum as input and outputs a normalized wave spectrum with the same wavenumber coordinates as the input.

The second stage (known as wave spectrum energy intensity retrieval), is dedicated to retrieving the specific wave spectrum intensity $SP_{\max}$ by combining the retrieved normalized wave spectrum $S_{0-1}(k_x, k_y)$. The ultimate 2-D wave spectrum is then obtained by directly multiplying the energy distribution $S_{0-1}(k_x, k_y)$ with the intensity $SP_{\max}$ of the wave spectrum.

The first stage is crucial as it facilitates the acquisition of features in the 2-D wave spectrum. To address the challenge of wave spectrum energy distribution retrieval, we consider employing the Generative Adversarial Nets (GANs) [33]. Unlike convolutional neural networks (CNNs), the GANs offer three distinct advantages for wave spectrum energy distribution retrieval. First, GANs can generate detailed 2-D wave spectrum features, going beyond the limitations of only extracting 1-D wave parameters. The second benefit is in the GAN's ability not only to memorize information from SAR imagettes but also to generate new, plausible information in line with the natural wave spectrum data distribution. Unlike the discriminative models like CNNs, the state of the art mutual guide strategy can automatically label the unlabeled data [34], [35]. GANs possess the capacity for imagination, allowing them to extend their understanding beyond the cutoff wavelength and retrieve wave spectra more comprehensively. The third advantage is the efficiency of training GANs without an absolute requirement for a vast amount of training data. The training data is augmented by the newly generated data during the training stage. In practical scenarios, where only a small set of SAR products and corresponding wave spectra are available, these three advantages highlight the capability of GANs as a promising algorithm for wave spectrum retrieval.

To use the superior ability of GANs for wave spectrum retrieval, we introduce an Energy Attention Conditional Generative Adversarial Net (EA-CGAN). The generator of the proposed EA-CGAN leverages extensive data to explore the intricate relationship between SAR spectra and corresponding wave spectra. In addition, an energy attention module is integrated to guide the EA-CGAN towards focusing more on valuable wave features. This enhancement allows the generator to establish a more effective transformation from normalized SAR spectra to normalized wave spectra.

In the second stage, we employ the XGBoost model to accomplish wave spectrum energy intensity retrieval. We validate our proposed two-stage retrieval strategy using a constructed dataset, consisting of Gaofen-3 wave mode products and ERA-5 2-D wave spectra. Furthermore, we provide the code for EA-CGAN and XGBoost, enabling the application of our method with various satellites. The code is available at https://github.com/YuxinFang21/WaveSpectrumRetrieval.

The rest of this article is organized as follows. Section II and III introduce the dataset used in the present study. Section IV outlines the two-stage wave spectrum retrieval strategy. Section V evaluates normalized wave spectra and ultimate wave spectra. Finally, Section VI concludes this article.

II. Data Catalog

To train the two-stage retrieval strategy that we proposed, we rely on two essential types of data: 1) SAR products; and 2) global ocean wave spectra products, all obtained for the same ocean regions within the same time windows. Our research data consists of collocated Gaofen-3 SAR wave mode HH polarimetric products and ERA-5 wave spectra data.

A. Gaofen-3 SAR Wave Mode Products

The Gaofen-3 satellite, equipped with a C-band (5.3 GHz) SAR sensor, operates in 12 imaging modes since August 2016. Specifically designed for ocean wave detection, the wave mode of Gaofen-3 SAR captures small SAR images known as imagettes every 50 km along the flight direction. These imagettes are configured with quad-polarimetric products, each covering a 5 km $\times$ 5 km area. The resolution of the azimuth direction is approximately 5.0 m and the range direction resolution is of 3.4 m. The preceding quality assessments have demonstrated a crosstalk accuracy of -35 dB for Gaofen-3. For our study, we compile Level-1 A HH polarimetric single-look complex (SLC) Gaofen-3 wave mode data spanning from 2016 to 2020. The retrieval dataset excludes SAR scenes without wave phenomena through the following operations: 1) deletion of power-saturated data based on "echoSaturation" values in annotation files; 2) exclusion of imagettes with low homogeneity [36]; and 3) removal of imagettes with ice, land, or islands.

B. ERA-5 2-D Wave Spectrum

Among the limited institutions capable of providing global 2-D wave spectra, the European Centre for Medium Range Weather Forecasts (ECMWF) is a reliable source. ECMWF's fifth-generation reanalysis, known as ERA-5 [37], provides precise estimations of 2-D wave spectra. These spectra result from a combination of abundant wave observations, advanced model estimation techniques, and proximity to data assimilation systems.

ERA-5 provides global wave spectra with 24 directions and 30 frequencies every 3 h. Direction bins start at 7.5° and increase by 15° until reaching 352.5, where 90° denotes the east direction. Frequency bins are distributed nonlinearly, starting with the first bin at 0.03453 Hz and finishing with the final bin at 0.6025 Hz. The bins increase according to the formula $f(n) = f(n-1) \times$

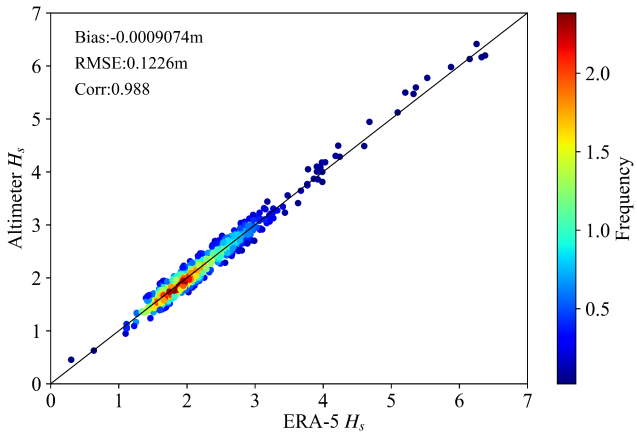

Fig. 1. Comparison of H_s calculated from ERA-5 wave spectra with H_s from SARAL altimeter. The color indicates the density of the data. The matched data number is 768.

1.1 for $n = 2, 3, \ldots, 30$. The ERA-5 wave spectra are accessible globally.

To validate the reliability of ERA-5 wave spectra, we compare the significant wave height H_s computed from ERA-5 with which obtained from the SARAL altimeter [38]. The H_s calculation equation for ERA-5 is demonstrated as follows:

$$H_s = 4\sqrt{\iint S(k_x, k_y)\, dk_x\, dk_y}. \tag{1}$$

Fig. 1 illustrates the comparison of H_s calculated from ERA-5 wave spectra with H_s from SARAL altimeter, with color indicating the data density. The results demonstrate the high quality and reliability of ERA-5 wave spectra.

C. Match-Up Datasets

Each SAR product is associated with a spatio-temporally matched ERA-5 wave spectra. The geographic position of the center pixel of the corresponding SAR imagette determines the geographic position of the ERA-5 wave spectra. The latitude and longitude grid is $0.1^\circ \times 0.1^\circ$. An one-hour window (+/– 0.5 h) is used between the matched SAR products and the ERA-5 wave spectra. In total, 11 312 data pairs are collected. Fig. 2 shows the global distribution of sample pairs. The histogram of significant wave heights calculated from ERA-5 wave spectra is depicted in Fig. 3, revealing that most samples have significant wave heights between 1.5 m and 2.5 m. All sample pairs are divided into a training set (65%) and a testing set (35%).

The implementation of our proposed two-stage strategy for wave spectra involves both aerial and reanalysis measurements. The ERA-5 wave spectra product supplements the energy information beyond the cutoff wavenumber. Therefore, the proposed wave spectrum inversion strategy develops an innovative data fusion scheme that combines satellite and reanalysis data to retrieve the complete wave spectra.

III. Data Preprocessing for 2-D Wave Spectra Retrieval

The data preprocessing stage involves several key steps, including the calculation of Gaofen-3 SAR cross spectra, computation of scalar features from Gaofen-3 SAR products, and transformation of the original ERA-5 wave spectra.

A. SAR Cross Spectra Calculation

The SAR cross spectra can effectively eliminate the spot noise and identity the wave propagation direction. According to the relevant process in [39], three sublooks $I_f^{(m)}(k,t)$ are created in the Fourier domain of SAR SLC imagettess using a Hamming window. Subsequently, three intensity imagettes $I^{(m)}(x)$ can be created from each separate sublook by computing the inverse fast Fourier transform (FFT) of the azimuth imagettes.

$$I^{(m)}(x) = \left| \frac{1}{(2\pi)^2} \int dk I_f^{(m)}(k,t) e^{-ikx} \right|^2 \tag{2}$$

where $m = [\ 1,2,3\ ]$. $I_f^{(m)}(k,t)$ is the Fourier domain of the corresponding sublook intensity imagettes $I^{(m)}(x)$. The cross-spectra are then calculated based on the individual look imagettes as follows:

$$P_s^{(m,n)}(\boldsymbol{k},\tau) = \frac{1}{\left\langle I^{(m)} \right\rangle \left\langle I^{(n)} \right\rangle} \left\langle I_f^{(m)}(k,0) I_f^{*(n)}(k,\tau) \right\rangle \tag{3}$$

where $\left\langle I^{(m)} \right\rangle$ is the mean imagettes intensity of the mth sublook. According to [25], the time separation between the pair of looks can be defined as follows:

$$\tau = \frac{\lambda R}{2 V_p V_f} \Delta B \tag{4}$$

where λ is the radar wavelength, R is the slant range to the center of the scene of interest, V_p is platform velocity, and ΔB represents the frequency difference between the centers of two looks.

The SAR imagettes cross-spectra with long-time separation are more discriminative than those with short time, as discussed in [40]. To enhance the determination of the wave propagation direction, $P_s^{(1,3)}(\boldsymbol{k},\tau)$ is employed for discriminative detection of the direction of wave propagation of SAR cross spectrum $P(\boldsymbol{k},\tau)$ in the subsequent section. Fig. 5(a) illustrates the results of cross-spectrum calculation, where a positive peak is observed at the North-East direction, indicating that the waves are heading in the North-East direction.

B. SAR Scalar Features

1) NRCS: The normalized radar cross section (NRCS) serves as an indicator of wave energy information related to short wave roughness [30]. In this work, NRCS is computed using the following formulation:

$$\sigma^0(\,\mathrm{dB}) = 10 \times \lg\left(\overline{DN}\right) - K. \tag{5}$$

Here, σ^0 represents the NRCS in dB, $\overline{DN}$ indicates the average value of DN, and $DN = I_s(qv/32767)^2$ represents the intensity of imagettes. The SLC SAR imagettes I_s are composed of

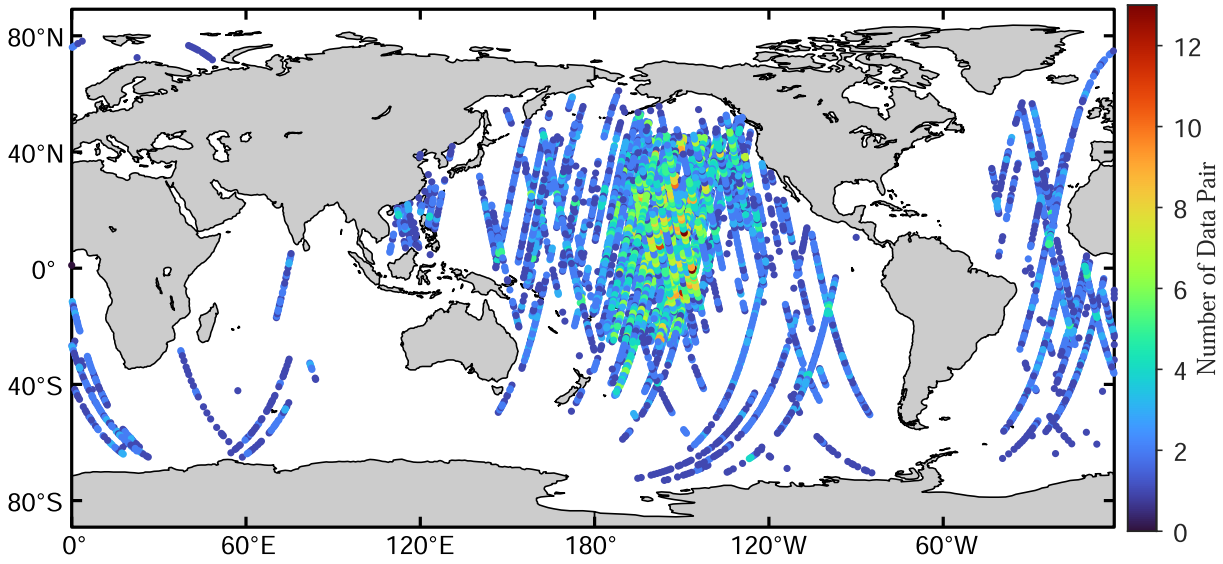

Fig. 2. Data density of Gaofen-3 wave mode imagettes from 2016 to 2020 in $2^\circ \times 2^\circ$ bins.

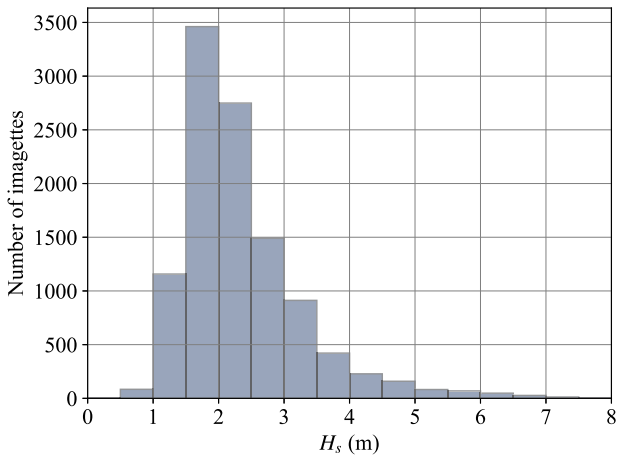

Fig. 3. Histogram of the ERA-5 H_s. The bin of the histogram is 0.5 m.

the real and imaginary channels, i.e., $I_s = I^2 + Q^2$. qv is the maximum qualified value, and K is the calibration constant, both of which are retained in the product annotation file.

2) cvar: The normalized imagettes variance ($cvar$) captures information about long waves and is commonly used in empirical H_s retrieval algorithms. The computation of $cvar$ for the Gaofen-3 is computed as follows:

$$cvar = \text{var}\left(\frac{DN - \langle DN\rangle}{\langle DN\rangle}\right). \tag{6}$$

3) Azimuth Cutoff Wavelength: The slight wave factors propagating close to the azimuth direction are generally distorted due to the velocity bunching of the SAR-ocean imaging mechanism. SAR cannot resolve the waves of which wavelengths are below the cutoff wavelengths λ_c. Theoretically, the azimuth cutoff wavelength (λ_c) is determined by the orbital velocity of ocean waves over the integration time along with the range-to-velocity ratio (β) of the SAR platform. Therefore, the value of λ_c normalized by β is a vital input feature for our models. The azimuth cutoff λ_c is calculated by fitting a Gaussian function C to the intercorrelation of SAR cross-spectrum [41]. The Gaussian function C is expressed as follows:

$$C(x) \sim \exp\left(-\pi^2 \frac{x^2}{\lambda_c^2}\right) \tag{7}$$

in which x is the spatial distance at the azimuth direction.

4) Incidence Angle: The incidence angle is also a crucial variable for significant wave height retrieval algorithms. In the Gaofen-3 wave mode, the incidence angle variable changes from 20° to 50°.

5) CWAVE Spectral Variables: 20 CWAVE spectral variables are calculated based on the SAR imagettes variance spectrum using an orthogonal basis set of 20 nondimensional variables [18].

C. ERA-5 Wave Spectrum Transformation

The ERA-5 wave spectra $S(f,\theta)$ are provided in frequency bins in polar coordinates, while the SAR cross spectra $P(k_x, k_y)$ are in Cartesian coordinates. Therefore, the ERA-5 wave spectra require to be transformed from frequency-direction to wavenumber domain [42]. The transformation from $S(f,\theta)$ to $S(k_x, k_y)$ is achieved in two steps [9]. First, we transform $S(f,\theta)$ to $S(k,\theta)$ using the formulation [9] as follows:

$$S(k,\theta) = \frac{S(f,\theta)g}{8\pi^2 f}\left[\tanh(kh) + \frac{kh}{\cosh^2(kh)}\right] \tag{8}$$

where k is the wavenumber and h is the finite water depth. According to the deep water gravity wave theory, $k = 4\pi^2 f^2/g$, with $g = 9.8\,\text{m/s}^2$ the gravitational acceleration. Then, $S(k_x, k_y)$ can be derived by using the Jacobian of (k,θ) with respect to (k_x, k_y) as follows:

$$S(k_x, k_y) = S(k,\theta)\frac{\partial(k,\theta)}{\partial(k_x, k_y)} = \frac{S(k,\theta)}{k}. \tag{9}$$

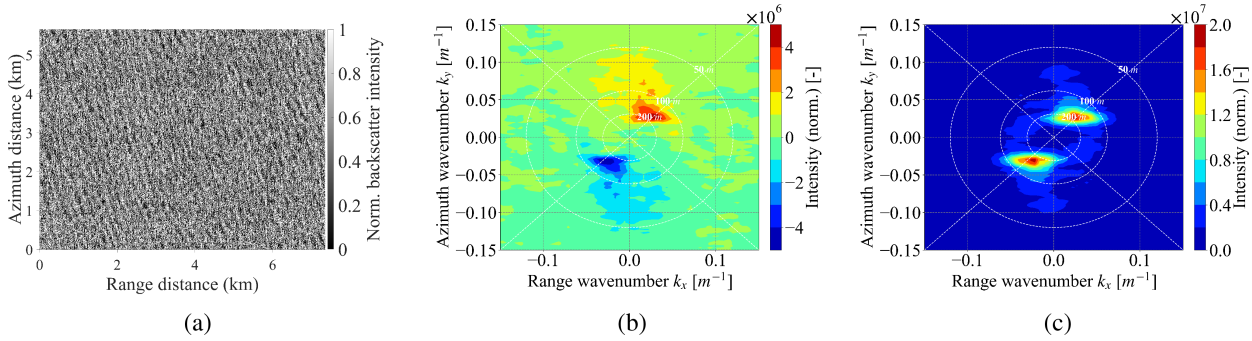

Fig. 4. (a) Normalized backscatter intensity of Gaofen-3 SAR wave mode sample. (b) The imaginary part of the crossspectrum. (c) The real part of the cross-spectrum.

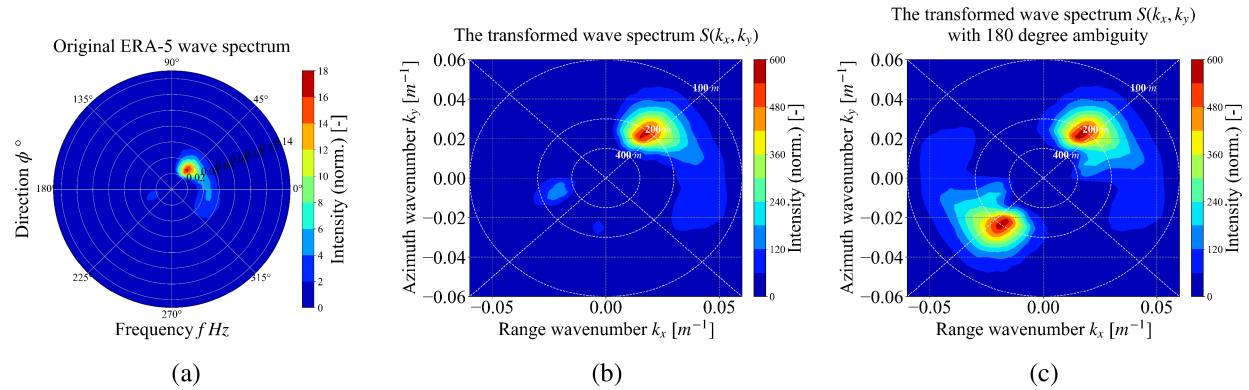

Fig. 5. Sample ERA-5 wave spectrum is matched with the Gaofen-3 SAR wave mode sample of Fig. 4. (a) The original wave spectrum provided by ERA-5. (b) The wave spectrum in Cartesian coordinate. (c) The wave spectrum with 180-degree ambiguity.

Linear interpolation is employed to convert the spatial resolution of both the SAR cross spectra $P(k_x, k_y)$ and ERA-5 wave spectra $S(k_x, k_y)$ to the same Cartesian coordinate (k_x, k_y). The SAR cross spectra have a 180° ambiguity, so the wave spectra also require the characteristic of 180° ambiguity. $S(k_x, k_y)$ with 180° ambiguity can be obtained as follows:

$$S(k_x, k_y) = S(k_x, k_y) + S(-k_x, -k_y). \tag{10}$$

Fig. 5 shows the relevant wave spectrum transformation results. Although this transformation strategy raises the question that two spectral energies differing by 180° may be superimposed, the peak wave direction is not influenced. In the subsection, we denote the $S(k_x, k_y)$ as the transformed wave spectra with 180° ambiguity. It is important to note that maintaining consistency by ensuring both input and output samples exhibit a 180° ambiguity significantly enhances the performance of the model presented.

D. Application of Features

To facilitate the wave spectrum energy distribution retrieval, the SAR cross-spectra and the transformed ERA-5 wave spectra are normalized to the [0–255] interval. Simultaneously, the 24 SAR features, including NRCS, normalized imagettes variance, azimuth cutoff wavelength, incident angle, and 20 CWAVE spectral parameters, are used for the wave spectrum intensity retrieval.

IV. Two Stage Retrieval Strategy for Retrieving 2-D Wave Spectra

The two-stage retrieval strategy is comprised of the wave spectrum energy distribution retrieval and the wave spectrum energy intensity retrieval. The overall process is illustrated in Fig. 6. In the first stage, known as the wave spectrum energy distribution retrieval, the objective is to produce the normalized wave spectra $S_{0-1}(k_x, k_y)$, reflecting the distribution of wave energy. The second stage (wave spectrum energy intensity retrieval) focuses on obtaining the specific wave spectrum intensity $SP_{\max}$ by combining the retrieved normalized wave spectra. The final wave spectra are therefore computed by directly multiplying the energy distribution and the intensity of the wave spectrum.

Section IV-A introduces the wave spectrum energy distribution retrieval using the proposed EA-CGAN. Section IV-B outlines the wave spectrum energy intensity retrieval using the XGBoost, and Section IV-C explains the calculation of the ultimate wave spectrum.

A. Wave Spectrum Energy Distribution Retrieval

To retrieve the normalized wave spectra $S(k_x, k_y)$ corresponding to the given normalized SAR cross spectra $P(\boldsymbol{k}, \tau)$, we employ a generative adversarial networks (GANs)-based model. This is because GANs [43], consisting of a generator and a discriminator, have demonstrated superior capabilities in generating new data.

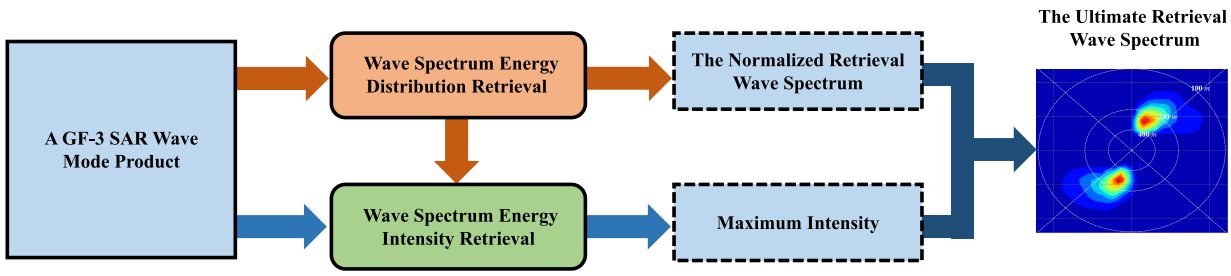

Fig. 6. Two-stage retrieval strategy for wave spectrum inversion.

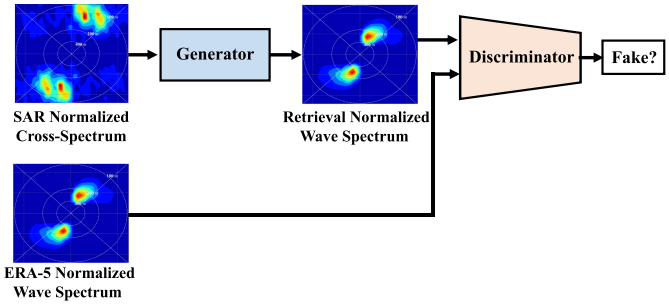

Fig. 7. Structure of proposed EA-CGAN.

In this study, the generator is designed to produce wave spectra that closely resemble ground truth wave spectra, i.e., ERA-5 wave spectra. Simultaneously, the role of the discriminator is to distinguish between the generated wave spectra and the ERA-5 wave spectra. Our emphasis is on training the generator of a GAN to create the normalized 2-D wave spectra. Initially, the GAN utilizes random noise as input to the generator, which is different from our task. To address this, we explore a potential method for wave spectrum energy distribution retrieval using a conditional generative adversarial net (CGAN).

In contrast to the initial model, the generator of the CGAN is trained with SAR spectrum data as inputs. These conditioning inputs serve as latent codes, addressing the uncontrollability observed in the initial GAN. To further leverage the superior capabilities of the CGAN and apply it to the wave spectrum retrieval task, we introduce an energy attention CGAN (EA-CGAN). The EA-CGAN is designed to establish a more attainable transformation from the normalized SAR spectra to the normalized wave spectra. An energy attention module is constructed to let the EA-CGAN prioritize the valuable wave energy information. In the following subsection, we outline the main structure of the EA-CGAN and explain the implementation of normalized wave spectrum inversion.

1) Structure of EA-CGAN: The structure of EA-CGAN is shown in Fig. 7. This model consists of an energy attention generator and a discriminator, both utilizing the convolution-BatchNorm-ReLu module form [44]. The role of the generator is to produce complete wave spectra that closely resemble the transformed ERA-5 wave spectra $S(k_x, k_y)$. On the other hand, the discriminator aims to distinguish the generated wave spectra from the ERA-5 transformed wave spectra $S(k_x, k_y)$.

These two components engage in an adversarial competition, wherein their abilities to generate authentic wave spectra and discriminate the generated counterparts are maximized. Following adversarial training, the generated wave spectra exhibit realistic characteristics and become indistinguishable from the real ERA-5 wave spectra when evaluated by the discriminator. The structure of the energy attention generator in the EA-CGAN is depicted in Fig. 8. During the training stage, the normalized SAR cross-spectrum passes through a series of layers that successively downsample until a bottleneck layer. At this point, the process is reversed, allowing all information from SAR cross spectra to flow through all the layers. Substantial spectrum information exists between the normalized SAR cross-spectra and the normalized wave spectra. For instance, the SAR cross spectra and wave spectra nearly share the direction of peak wave propagation. To leverage this information effectively and in line with the architecture of a "U-Net" [45], skip connections (depicted as red dotted lines in Fig. 8) are added to facilitate the sharing of spectrum information. Specifically, the skip associations are added between each layer i and layer $n-i$, where n is the total number of layers. In this arrangement, each skip association combines all features at layer i with those at layer $n-i$.

The wave spectrum energy values are quite small at specific directions and wavenumbers, resulting in near-zero pixel values in both the SAR cross-spectrum and wave spectrum. Consequently, the generator needs to pay more attention to pixels that contain valuable energy information. To address this, an energy attention module is introduced in each convolution block to guide the generator in focusing on locations with significant wave spectrum energy, as illustrated in Fig. 9. Given an intermediate feature map, the spectrum energy attention module generates attention maps along the spatial dimension channel. Subsequently, the spectrum energy attention map is multiplied by the input feature map to adjust feature refinement.

2) Loss Functions: The SAR cross-spectra, corresponding ERA-5 wave spectra, and retrieval wave spectra are denoted as P, S, and S_G, respectively. The energy attention generator and the discriminator of EA-CGAN optimize themselves through two loss functions L_1 and L_G for the generator, and L_D for the discriminator. The generator G aims to generate a wave spectrum S_G that closely resembles the ERA-5 wave spectrum S. Two loss functions are employed to evaluate the similarity on two aspects. The L_1 norm loss function is given by

$$L_1 = |S_G - S|. \tag{11}$$

The L_1 norm loss function provides an objective similarity measure between S_G and S. The L_G loss obtained from the

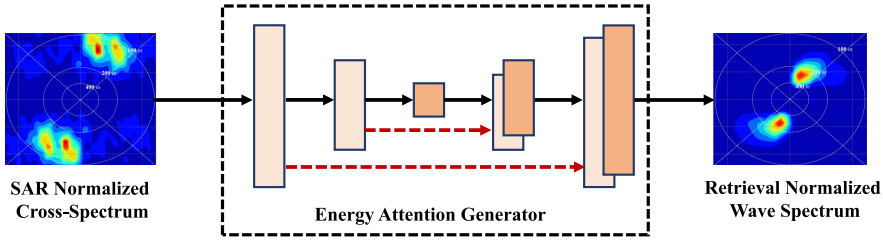

Fig. 8. Structure of the energy attention generator.

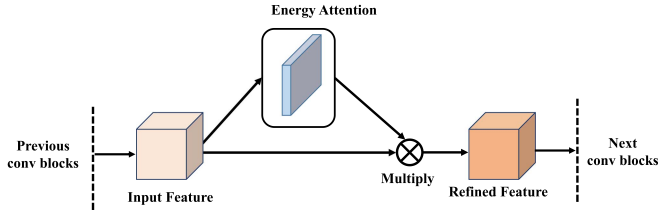

Fig. 9. Energy attention module.

discriminator measures the similarity between S_G and S.

$$L_G = E[\log(1 - D(S_G, S))]. \tag{12}$$

The term $D(S_G, S)$ calculated from the discriminator D is a dissimilarity score that estimates the dissimilarity between S_G and S with respect to the value in the interval of 0–1. The term $1 - D(S_G, S)$ indicates the similarity by the discriminator D. Optimizing L_G to minimization boosts the generator G to generate the retrieval wave spectrum, which is close to the ERA-5 wave spectrum, and cheats the discriminator D as far as possible. To make D effectively discriminate the generated wave spectrum S_G from the ERA-5 wave spectrum S, the loss function for optimizing D is expressed as follows:

$$L_D = E[\log D(S_G, S)] \tag{13}$$

with L_D measuring the different score of D. We maximize the loss L_D to train the discriminator. The entire loss function of training the EA-CGAN is formed by summing the loss functions (11) and (12) to train G and the loss function (13) to train D. The entire loss function is

$$L_{\text{CGAN}} = L_G + L_D + \alpha L_1 \tag{14}$$

where α is an empirical scaling variables. We individually minimize and maximizing the loss L_{CGAN} to train G and D as follows:

$$(G_*, D_*) = \arg \min_G \max_D L_{\text{CGAN}}. \tag{15}$$

First, the values of G are updated by minimizing the sum of (11) and (12). Then, the values of D are updated by maximizing (13). The min-max training process concerning (15) is adversarial and can be considered a race between G and D.

Finally, the discriminator is unable to be differentiated between generated wave spectra and ERA-5 wave spectra. The Adam optimizer [46] is utilized to implement the minimization and maximization process.

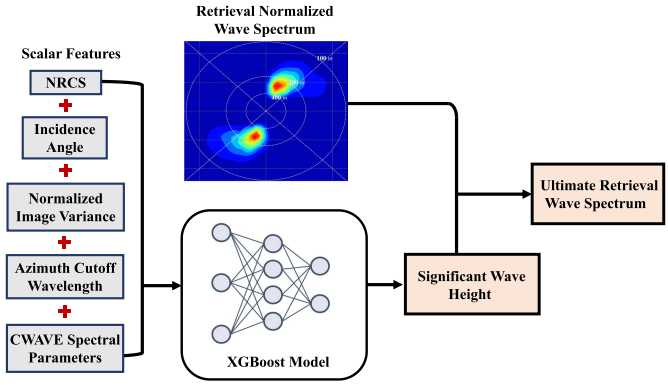

Fig. 10. Framework of wave spectrum energy intensity retrieval.

3) Wave Spectrum Energy Distribution Retrieval via Energy Attention Generator: Following the adversarial training stage, the energy attention generator is extracted for achieving the wave energy distribution retrieval. The generator G_* revised after the adversarial training stage is capable of directly generating the complete corresponding normalized wave spectra without relying on prior information. From the perspective of wave spectrum retrieval, the generator establishes a direct and intricate nonlinear transformation from the SAR cross-spectra to the wave spectra.

B. Wave Spectrum Energy Intensity Retrieval

This section introduces the process of wave spectrum energy intensity retrieval. The overall framework is shown in Fig. 10. First, the machine learning algorithm XGBoost is implemented to retrieve the H_s from 4 scalar variables and 20 CWAVE spectral parameters. The XGBoost has been successfully applied to fit H_s from several SAR features [30]. The XGBoost model can be expressed as follows:

$$\hat{y}_i = \sum_{k=1}^{K} f_k(x_i), f_k \in F(i = 1, 2, \ldots n) \tag{16}$$

in which F is a list of decision trees, $\hat{y}_i$ denotes the forecast H_s, and n denotes the data number. XGBoost is trained by minimizing the objective function shown as follows:

$$L_{\text{Obj}} = L + \Omega. \tag{17}$$

In this context, L evaluates the bias between $\hat{y}_i$ and y_i which denotes the H_s calculated from ERA-5 wave spectra. The additional regularization term Ω decreases the complexity of the

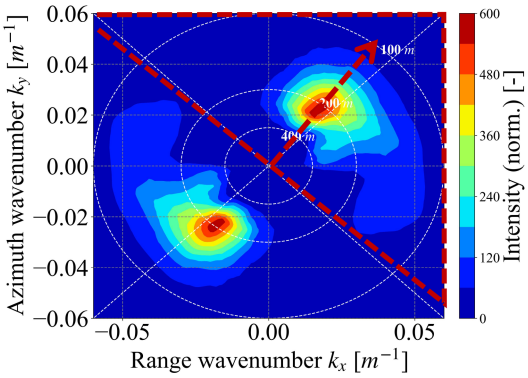

Fig. 11. Process of removing 180° ambiguity for the retrieval wave spectrum retrieved from the sample in Fig. 4. The red dashed box represents the ultimate retrieval wave spectrum.

XGBoost to avoid overfitting. Next, we integrate the retrieved H_s with the corresponding generated normalized wave spectrum to calculate practical intensity values. The lowest intensity of the practical wave spectrum is considered as zero, as wave energy is negligible at certain wavenumbers. Therefore, the practical wave spectrum can be represented as follows:

$$S(k_x, k_y) = SP_{\max} S_{0-1}(k_x, k_y). \tag{18}$$

Once the maximum intensity $SP_{\max}$ is determined, the intensity values for the entire practical wave spectrum are established. Based on (1), the maximum intensity $SP_{\max}$ is expressed as follows:

$$SP_{\max} = \frac{H_s^2}{16 \iint S_{0-1}(k_x, k_y) dk_x dk_y}. \tag{19}$$

C. Ultimate Directional Wave Spectra

The directional wave spectra obtained using (18), while retaining a 180° ambiguity postcalculation, require only one half for analysis. To resolve this ambiguity and enhance directional resolution aided by the temporal separation between individual imagettes [40], the imaginary part of the cross-spectrum $P_s^{(1,3)}(\boldsymbol{k}, \tau)$ between individual looks 1 and 3 is employed. A positive peak in this imaginary cross-spectrum identifies the wave propagation direction and is considered as the directional wave spectrum's center point. For instance, in Fig. 4, a positive peak is observed in the North-East direction. To remove the 180° ambiguity, the positive peak of the imaginary part is selected as the center of the ultimate directional wave spectrum. Subsequently, the complete 180° range of the retrieval wave spectrum is extracted, as depicted in Fig. 11, where the red dashed box represents the ultimate retrieval wave spectrum.

The overall wave spectrum two-stage retrieval strategy is shown in Algorithm 1.

Algorithm 1 delineates our proposed two-stage retrieval strategy for retrieving complete wave spectra from Gaofen-3 SAR products, eliminating the need for prior information. Depending on specific requirements, the wave spectra in the wavenumber $k_x - k_y$ domain can be transformed back to the frequency-direction formulation using (8) and (9).

Algorithm 1: The Two-Stage Retrieval Strategy.

Inputs: SAR cross spectra $P(k_x, k_y)$, SAR scalar features.

1) The normalized wave spectra $S_{0-1}(k_x, k_y)$ are generated by the energy attention generator G from the SAR cross spectra.
2) The significant wave heights H_s are estimated from SAR scalar features via XGBoost.
3) Combining the H_s and retrieval normalized wave spectra $S_{0-1}(k_x, k_y)$, the maximum intensity $SP_{\max}$ for each retrieval wave spectrum is obtained.
4) The complete retrieval wave spectra $S(k_x, k_y)$ are calculated by $S(k_x, k_y) = SP_{\max} \times S_{0-1}(k_x, k_y)$.
5) After removing the 180-degree ambiguity, the ultimate wave spectrum is obtained.

Outputs: Retrieval Wave Spectra $S(k_x, k_y)$

V. 2-D Retrieval Wave Spectrum Evaluation

Our wave spectrum two-stage retrieval framework is implemented using the PyTorch framework on CentOS 7.3. The EA-CGAN is trained with SGD, employing a learning rate of 0.001, a momentum of 0.95, a constant LR schedule, and a batch with a size of 32. The training consists of 150 iterations. The training session runs for 150 epochs with a batch size of 8. The learning rate of the Adam optimizer starts from the initial 0.0005, using the ascending decay as well as the rate of 0.96. The XGBoost is trained with an estimator number of 200, max depth of 50, and learning rate of 0.05.

A. Qualitative Evaluation of Normalized 2-D Wave Spectra

The pivotal aspect of the proposed two-stage retrieval strategy is the retrieval of normalized wave spectra. While the normalized wave spectra are represented in the range of 0–255 rather than practical values, various wave parameters such as mean wave period, peak period, and peak direction can be derived based on these normalized wave spectra. The energy intensity retrieval stage does not alter the shape of the normalized wave spectra, but only adjusts the wave energy values for each wavenumber. In this section, the retrieved normalized wave spectra, $S_{0-1}(k_x, k_y)$, from the first stage are evaluated against the ERA-5 normalized wave spectra using a 2-D spectrum similarity measurement.

So far, only a few evaluation criteria can accurately assess the similarity of 2-D wave spectra. In order to rigorously evaluate the performance of our proposed method in retrieving normalized wave spectra, we utilize a set of widely recognized evaluation metrics commonly employed for measuring imagettes similarity. These metrics serve to quantitatively measure the degree of similarity and dissimilarity between the 2-D normalized ERA-5 wave spectra and the 2-D normalized retrieval wave spectra. Specifically, four key evaluation parameters are employed. The relevant quantitative evaluation metrics are presented as follows.

1) *Peak Signal-to-Noise Ratio (PSNR):* PSNR is a metric commonly used for assessing image quality, and it can

TABLE I
QUALITATIVE EVALUATION RESULTS FOR ENERGY DISTRIBUTION RETRIEVAL IN FOUR SEA STATES

Sea states	Sample number	Similarity evaluation metrics			
		SSIM	PSNR(dB)	RMSE	$\rho(A,B)$
$H_s > 4.5$ m	152	0.9250	33.14	6.321	0.9027
4.5 m$\geq H_s > 3$ m	693	0.9177	33.05	7.132	0.8869
3 m$\geq H_s > 1.5$ m	2839	0.9102	32.93	7.024	0.8561
$H_s \leq$1.5 m	340	0.8435	29.31	9.842	0.8399
Total test samples	4024	0.9064	32.65	7.254	0.8576

also indicate image similarity. Computed as the mean squared error between the signal (ERA-5 wave spectra) and the noise (differences between ERA-5 and retrieval normalized wave spectra), a high PSNR value indicates a small mean squared error in the retrieval result, thereby reflecting a high similarity between the retrieval and ERA-5 normalized wave spectra.

2) *Structure Similarity Index Measure (SSIM):* SSIM quantifies differences in peak wave energy, contrast, and wave energy distribution between the normalized retrieval wave spectra and normalized ERA-5 wave spectra. Ranging between 0 and 1, a higher SSIM value indicates a closer approximation of the normalized retrieval wave spectra to the normalized ERA-5 wave spectra.
3) *Root Mean Square Error (RMSE):* RMSE is an objective evaluation indicator calculated by the pixel-level error between the normalized retrieval wave spectrum and the normalized ERA-5 wave spectrum. Reflecting the degree of difference between them, a small RMSE represents a superior result where the normalized retrieval wave spectra closely match the normalized ERA-5 wave spectra.
4) *Linear (Bravais–Pearson) Correlation Coefficient ρ:* ρ is employed to estimate the correlation between the retrieval spectra and the reference ERA-5 spectra. It is represented as follows:

$$\rho(A,B) = \sum_{i,j=1}^{N} (A_{ij} - \mu_A)(B_{ij} - \mu_B) \cdot \frac{1}{\sqrt{\left(\sum_{i,j=1}^{N} (A_{ij} - \mu_A)^2\right)\left(\sum_{i,j=1}^{N} (B_{ij} - \mu_B)^2\right)}} \tag{20}$$

where A_{ij} and B_{ij} indicate the energy of retrieval wave spectrum and the ERA-5 wave spectrum on wavenumbers $k_{ij}(i,j = 1,\ldots,N)$. k_{ij} represents the wavenumber with the interval of $\Delta k = 0.001$ and the range of [0.005, 0.2]. μ_A and μ_B denote the average values for A_{ij} and B_{ij}, separately.

Table I presents the results of qualitative similarity evaluations across four sea states: $H_s \leq 1.5$ m, 1.5 m $< H_s \leq 3$ m, 3 m $< H_s \leq 4.5$ m, and $H_s > 4.5$ m. The SSIM, PSNR, and RMSE scores for the entire test dataset demonstrate sufficient performance in terms of image similarity [47], affirming the proficient generative capability of the proposed energy attention generator. More specifically, the SSIM, PSNR, and $\rho(A,B)$ values for the retrieval results in three sea states ($H_s > 1.5$ m) exceed 0.9, 30 dB, and 0.85, respectively. In addition, the RMSE values for the retrieval results in these states (where $H_s > 1.5$ m) are consistently below 7.5.

When comparing the four sea states, the retrieval samples in the highest sea state ($H_s > 4.5$ m) exhibit the most significant average scores across all three evaluation criteria. In contrast, the retrieval samples in the lowest sea state ($H_s \leq 1.5$ m) demonstrate inferior average scores, likely attributed to the poor signal-to-noise ratio of SAR spectra in this lowest sea state. In general, the influence of noise in SAR cross-spectra is more pronounced in low sea states, despite the reduction of speckled noise through cross-spectrum processing. The noise energy levels in low sea states are relatively improved, leading to a more challenging scenario where noise and useful wave spectra information become intertwined and indistinguishable. As a result, the energy attention generator of the EA-CGAN may misconstrue irrelevant noise information as useful wave spectra information, generating inaccurate wave information from noise signals in SAR spectra. Fig. 12 illustrates histograms of SSIM, PSNR, and $\rho(A,B)$ for the retrieved energy distribution results. While the majority of samples exhibit satisfactory SSIM, PSNR, and NRMSE results, a subset of extreme conditional retrieval outcomes can impact the overall retrieval performance.

Figs. 13 and 14 present eight specific examples across four sea states, providing a detailed exploration of the effectiveness of the energy distribution retrieval model. Each row corresponds to a group of time-space-matched samples. The main wave direction of each sample is obtained from the corresponding SAR cross-spectrum which is as explained in Section IV-C. Visually, these 2-D normalized retrieval examples exhibit a high degree of consistency with their respective 2-D normalized ERA-5 wave spectra in terms of relative energy values and distribution. For some SAR products that have distinctive wave features, the proposed EA-CGAN demonstrates robust capabilities in retrieving complete wave spectra, as shown in Figs. 13, 14(b), and (d). In Fig. 13(c), EA-CGAN generates additional wave information present in the SAR cross-spectrum but absent in the ERA-5 wave spectrum. Even for SAR products lacking distinct

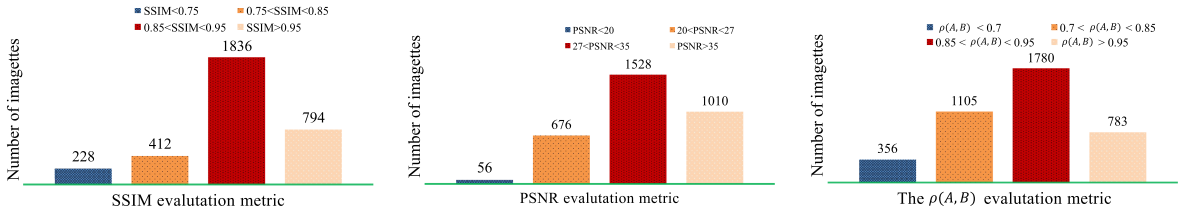

Fig. 12. Histograms of PSNR, SSIM, and linear correlation coefficient $\rho(A, B)$.

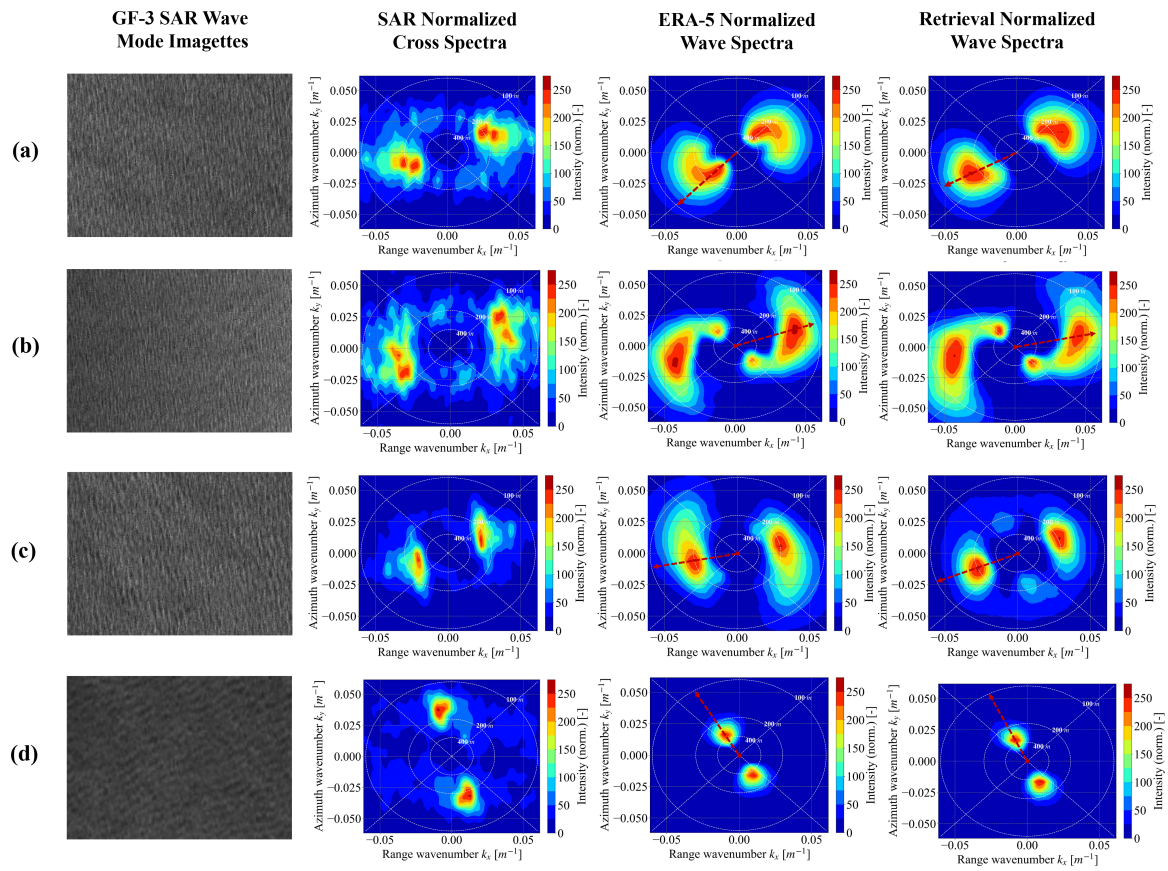

Fig. 13. Retrieval normalized wave spectrum results on two comparably high sea states. (a)$H_s = 5.35$ m. (b) $H_s = 5.23$ m. (c) $H_s = 4.43$ m. (d) $H_s = 4.36$ m.

wave features, as observed in Fig. 14(c) and (d), our proposed EA-CGAN demonstrates its ability to extract valuable wave information from the SAR cross-spectrum, which may contain complex noise signals.

The wave propagation direction is a vital parameter that can be roughly recognized from SAR imagettes and SAR cross-spectra. In the presented examples, the wave propagation direction in 2-D normalized retrieval wave spectra is observed to be closer to that in SAR cross-spectra than in 2-D normalized ERA-5 wave spectra, particularly evident in Fig. 13(a). These observations suggest that the generator of EA-CGAN successfully establishes a direct transformation from SAR normalized cross-spectra to the corresponding normalized wave spectra.

In summary, the evaluation results confirm the capability of the energy distribution wave spectrum retrieval model to effectively retrieve normalized wave spectra for most sea states.

B. Qualitative Evaluation of the Ultimate Wave Spectra

Following the confirmation of the effectiveness of the EA-CGAN in the first stage, we proceed to evaluate the ultimate directional wave spectra $S(k_x, k_y)$ with a focus on the omni-directional wave spectra $S(k)$ and several practical wave parameters. The ultimate directional wave spectra are acquired according to the process in Section IV-C. Prior to the evaluation, the $S(k_x, k_y)$ is transformed to $S(k, \theta)$ using (9).

1) Qualitative Evaluation of the Omni-Directional Wave Spectra: The omni-directional wave spectra $S(k)$ are determined by integrating $S(k, \theta)$ in wave propagation direction, expressed as

$$S(k) = \int_0^{2\pi} S(k, \theta) d\theta. \tag{21}$$

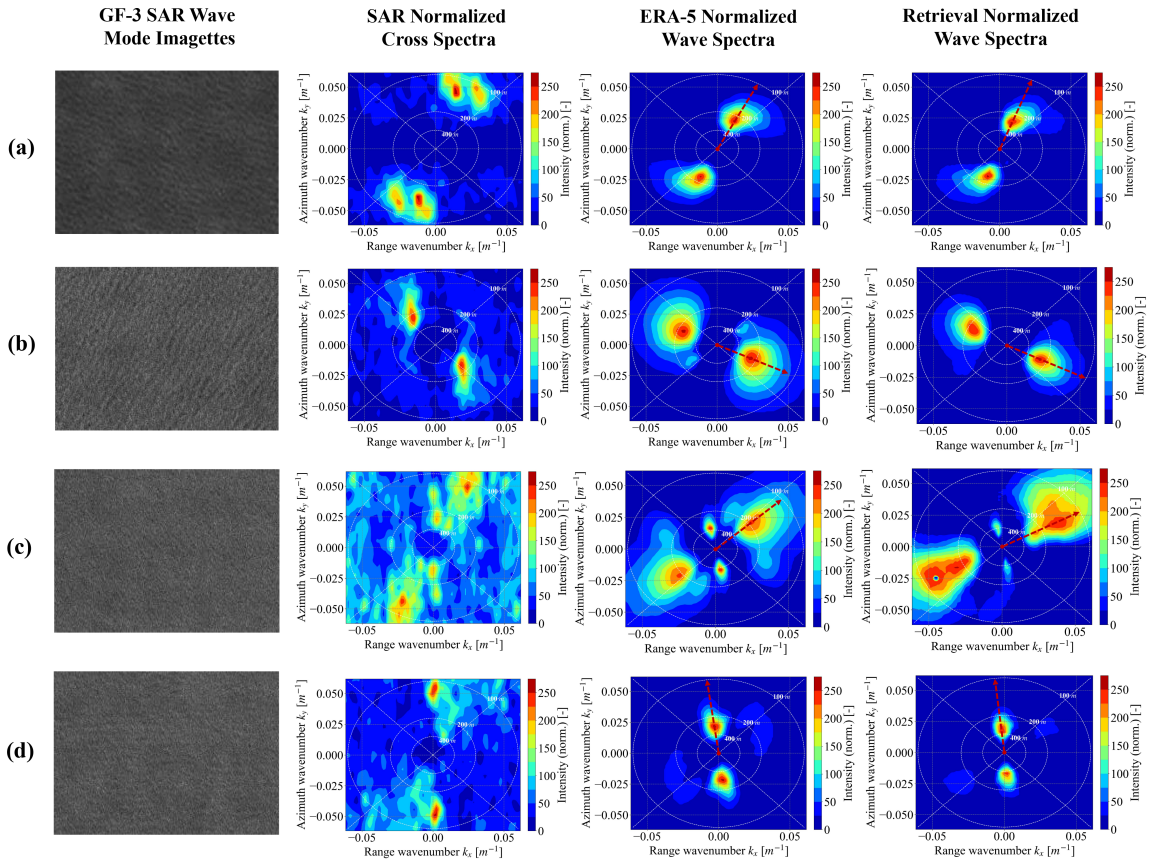

Fig. 14. Retrieval normalized wave spectrum results on two comparably low sea states. (a) $H_s = 1.78$ m. (b) $H_s = 2.18$ m. (c) $H_s = 0.91$ m. (d) $H_s = 1.40$ m.

Three evaluation indicators (i.e., the linear correlation coefficient ρ in terms of one dimension, the relative integral error ΔE, the peak wavenumber error Δk_{p1}) are employed to quantitatively assess the retrieval omni-directional normalized wave spectra.

The linear (Bravais–Pearson) correlation coefficient ρ for the omnidirectional wave spectrum similarity measurement is defined as follows:

$$\rho(A,B) = \frac{\sum_{i=1}^{N}(A_i-\mu_A)(B_i-\mu_B)}{\sqrt{\left(\sum_{i=1}^{N}(A_i-\mu_A)^2\right)\left(\sum_{i=1}^{N}(B_i-\mu_B)^2\right)}} \tag{22}$$

where A_i and B_i indicate the mean retrieval wave spectra and the mean ERA-5 wave spectrum discretized on wavenumbers $k_i (i = 1, \ldots, N)$. k_{ij} represents the wavenumber with the interval of $\Delta k = 0.001$ and the range of [0.005, 0.2]. μ_A and μ_B denote the average values for A_i and B_i, respectively. The relative integral error ΔE quantitatively assesses the dissimilarity between the ERA-5 omnidirectional spectra and the retrieval omnidirectional wave spectra [48]. ΔE is defined as follows:

$$\Delta \mathrm{E} = \frac{\sum_{i=1}^{N} A_i \Delta k_{Ai} - \sum_{i=1}^{N} B_i \Delta k_{Bi}}{\sum_{i=1}^{N} B_i \Delta k_{Bi}} \times 100\% \tag{23}$$

where A_i and B_i denote the average retrieval wave spectra and the mean ERA-5 wave spectra on wavenumbers k_i $(i = 1, \ldots, N)$, respectively. The peak wavenumber error $\Delta kp1$ estimates the dissimilarity on peak wavenumber. It is represented as follows:

$$\Delta k_{p1} = \frac{k_{p1\_A} - k_{p1\_B}}{k_{p1\_B}} \times 100\% \tag{24}$$

where k_{p1_A}, k_{p1_B} indicate the wavenumber with the maximum energy.

Fig. 15 demonstrates the retrieval of omni-directional spectral results in four sea states. The sea state, $3\,\mathrm{m} \geq H_s > 1.5\,\mathrm{m}$, achieves the most outstanding fitting with the greatest $\Delta E = -1.2\%, \Delta k_{p1} = 4.03\%$, but an inferior $\rho = 0.94$. For the two comparably high sea states ($H_s > 4.5\,\mathrm{m}$ and $4.5\,\mathrm{m} \geq H_s > 3\,\mathrm{m}$), the retrieved omni-directional spectra demonstrate apparent underestimation when the wavenumber is lower than 0.75 rd/m. In addition, a small overestimation appears when the wavenumber exceeds 0.75 rd/m. For the sea state $H_s \leq 1.5$ m, the retrieval results show substantial overestimation with $\Delta E = -15.2\%, \Delta k_{p1} = 7.87\%$, and $\rho = 0.97$. These deviations in the retrieval of omni-directional wave spectra are mainly caused by the poor fitting performance of H_s by the XGBoost model. The H_s estimation results via XGBoost also exhibit overestimation and underestimation in the lowest and highest sea states.

In summary, the retrieval of omni-directional spectra shows superior consistency with ERA-5 in medium sea states (4.5 m $\geq H_s >$ 3 m and 3 m $\geq H_s >$ 1.5 m). In extreme sea states

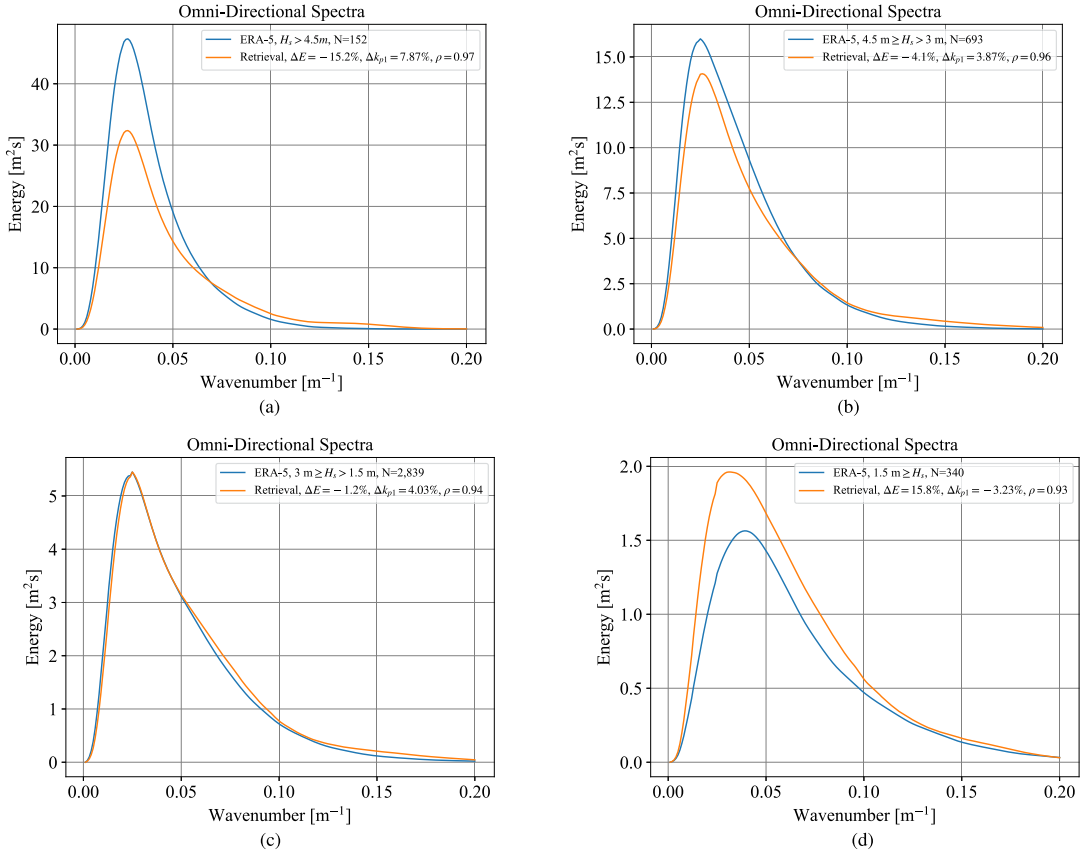

Fig. 15. Retrieval omni-directional spectra results for four sea states. N indicates the number of samples in the corresponding sea state. (a) $H_s > 4.5$ m. (b) 4.5 m $\geq H_s >$ 3 m. (c) 3 m $\geq H_s >$ 1.5 m. (d) 1.5 m $\geq H_s$.

($H_s > 4.5$ m and $H_s \leq 1.5$ m), the consistencies, while inferior, are acceptable. The variation tendency of retrieval omni-directional spectra and ERA-5 omni-directional spectra in four sea states are similar, which indicates that the EA-CGAN model achieves superior performance. Improving the performance of the H_s retrieval model can enhance the effectiveness of the omni-directional spectra fitting because the main difference is derived from specific intensity values.

2) Qualitative Evaluation of Ocean Wave Parameters: The evaluation of the energy intensity retrieval model extends to practical wave parameters computed from the ultimate retrieval wave spectra. These parameters include peak wave period, significant wave height, mean wave period, and peak direction. To evaluate the energy intensity retrieval model qualitatively, three standard metrics are employed, which are the mean bias (Bias), root mean square error (RMSE), and correlation coefficient (Corr).

The peak wave period (PP) is defined as follows:

$$PP = \frac{2\pi}{\sqrt{gk_{\max}}} \tag{25}$$

where $k_{\max}$ denotes the wavenumber of the peak wave energy. The peak wave direction denotes the direction of the peak wave energy. Due to the 180° ambiguity of the ultimate retrieval wave spectrum, two peak wave directions with an interval of 180° are captured. The peak wave direction, closer to the positive peak direction of the imaginary part of the corresponding SAR cross-spectrum, is considered as the ultimate peak wave direction. The positive peak direction of the imaginary indicates the practical peak wave direction so that the largest difference between the retrieval and ERA-5 peak wave direction is 90°. We calculate the significant wave height (H_s) using the following formula (1). Accurate representation of mean ocean wave periods is essential for various practical applications, and different formulations exist for this purpose. One simplest representation, T_{m01}, is defined as

$$T_{m01} = m_0/m_1. \tag{26}$$

In addition, the frequently used zero up-crossing period, denoted as T_{m02}, is expressed as

$$T_{m02} = m_0/m_2. \tag{27}$$

The energy wave period is defined by

$$T_{m-10} = m_{-1}/m_0, \tag{28}$$

where the moments m_k are given by

$$m_n = \int_0^{2\pi} \int_{f_{\min}}^{f_{\max}} f^n S(f,\theta) df d\theta. \tag{29}$$

These different mean ocean wave periods have been used in various contexts, with T_{m02} being widely used in ocean engineering, and T_{m-10} commonly employed in wave energy applications [49].

TABLE II
WAVE PARAMETER RETRIEVAL RESULTS ARE SUBJECT TO COMPARING THE RETRIEVAL WAVE SPECTRA AND ERA-5 WAVE SPECTRA

Sea state parameters	Sea states	Sample number	Evaluation metrics		
			Bias	RMSE	Corr
Significant wave height	$H_s > 4.5$ m	152	–0.6533	0.8970	0.6531
	4.5 m$\geq H_s > 3$ m	693	–0.1945	0.4617	0.6074
	3 m$\geq H_s > 1.5$ m	2,839	0.02497	0.3046	0.7187
	$H_s \leq$1.5 m	340	0.1696	0.2237	0.5857
	Total test samples	4,024	–0.02626	0.3686	0.9147
Peak period	$H_s > 4.5$ m	152	–0.2005	1.008	0.7409
	4.5 m$\geq H_s > 3$ m	693	–0.1952	1.231	0.8019
	3 m$\geq H_s > 1.5$ m	2,839	–0.1823	1.580	0.7419
	$H_s \leq$1.5 m	340	0.3735	1.703	0.6476
	Total test samples	4,024	0.1382	1.519	0.7492
Peak direction	$H_s > 4.5$ m	152	–0.8757	20.41	0.9587
	4.5 m$\geq H_s > 3$ m	693	2.2830	23.39	0.9510
	3 m$\geq H_s > 1.5$ m	2,839	0.030	23.09	0.9670
	$H_s \leq$1.5 m	340	–6.748	25.93	0.9645
	Total test samples	4,024	–0.1892	23.30	0.9647
Mean period T_{m01}	$H_s > 4.5$ m	152	–0.4194	0.6257	0.7539
	5 m$\geq H_s > 3$ m	693	–0.2372	0.6349	0.8410
	3 m$\geq H_s > 1$ m	2,839	–0.1503	0.6366	0.8227
	$H_s \leq$1 m	340	0.1539	0.4114	0.6827
	Total	4,024	–0.1497	0.6199	0.8305
Zero upcrossing period T_{m02}	$H_s > 4.5$ m	152	–0.4541	0.6450	0.7356
	5 m$\geq H_s > 3$ m	693	–0.2611	0.6524	0.8252
	3 m$\geq H_s > 1$ m	2,839	–0.1592	0.6344	0.8071
	$H_s \leq$1 m	340	0.1324	0.3796	0.6754
	Total samples	4,024	0.1633	0.6206	0.8169
Energy period T_{m-10}	$H_s > 4.5$ m	152	–0.3392	0.5928	0.7752
	5 m$\geq H_s > 3$ m	693	–0.1906	0.6048	0.8654
	3 m$\geq H_s > 1$ m	2,839	–0.1292	0.6360	0.8487
	$H_s \leq$1 m	340	0.2042	0.4869	0.6938
	Total samples	4,024	0.1195	0.6178	0.8519

Table II presents the comprehensive evaluation results for the retrieval of six key wave parameters, while Fig. 16 illustrates scatter plots showing these parameters. Notably, samples from two moderate sea states (4.5 m $\geq H_s >$ 3 m, 3 m $\geq H_s >$ 1.5 m), constituting a substantial portion of the total dataset, exhibit superior scores across all three evaluation indices for six wave parameters. The evaluation of significant wave height (H_s) across the entire dataset demonstrates satisfactory results in terms of three metrics. Samples from the lowest sea state yield comparatively lower evaluation scores, likely influenced by the smaller sample size.

The peak period evaluation results in Table II indicate a reasonable overall correlation of 0.7492, accompanied by an RMSE of 1.519 s and a Bias of 0.1382 s. The minimal observed peak period is approximately 7.1 s, corresponding to a wavelength of 78.5 m. It is important to note that identifying the peak period depends on accurately determining the peak wavenumber pixel in the wave spectrum. As the peak wavenumber value drops and the peak period increases, the prediction error for the peak period also rises due to the resolution of peak wavenumber pixels. Consequently, when dealing with high peak periods, even slight shifts in pixel positions can cause substantial inaccuracies in estimating the peak period. This factor inherently limits the accuracy of peak period retrieval, as illustrated by Fig. 16(a), where a single high peak period corresponds to several retrieved peak periods. The sea state of 4.5 m $\geq H_s >$ 3 m demonstrates the most favorable performance, achieving a correlation of 0.8019, an RMSE of 1.231 s, and a Bias of -0.1952 s. Conversely, the lowest sea state ($H_s \leq 1.5$ m) yields the least satisfactory results. This difference is primarily due to the prevalence of swell

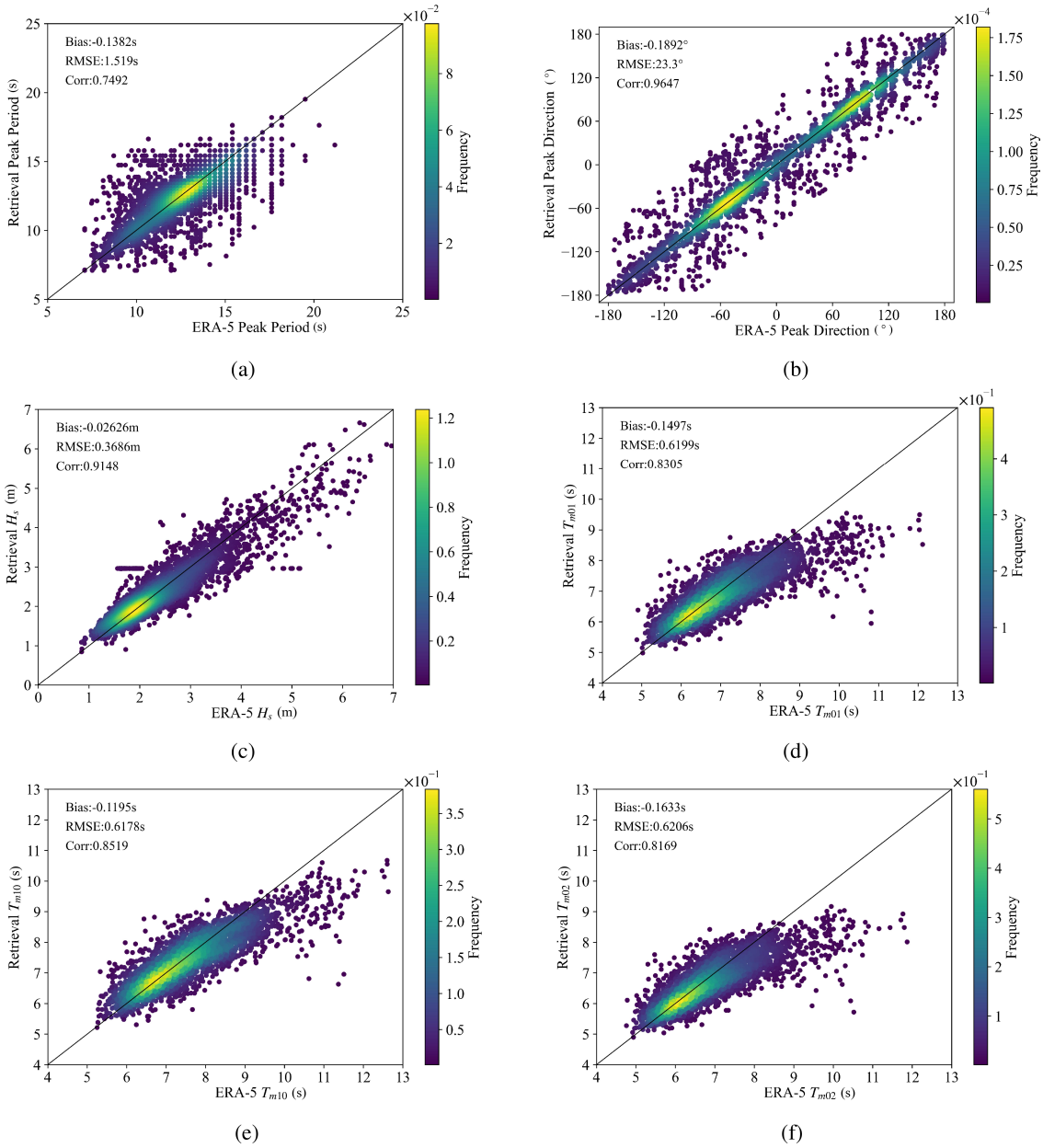

Fig. 16. Scatter results of retrieval ocean wave six parameters: (a) peak period, (b) peak direction, (c) significant wave height H_s, (d) mean period T_{m01}, (e) zero up-crossing period T_{m10}, and (f) energy wave period T_{m02}. The data number is 4,024.

waves in the lowest sea state, characterized by extended peak periods. Waves with larger peak periods give greater challenges, resulting in more significant errors compared to waves with shorter periods.

Table II further highlights the satisfactory performance of the three practical wave period parameters across total test samples, with Bias values below 0.20 s, RMSE values below 0.65 s, and correlation coefficients above 0.8. The lowest and highest sea states exhibit comparatively lower correlation scores on the three period parameters when compared to the moderate sea states, a trend consistent with the omni-directional wave spectrum results. This difference is related to the limited availability of extreme sea state data, contributing to a reduced performance evaluation. In addition, it should be mentioned that longer wave periods are typically associated with more intense events and high sea states [18], which contain long-winded sea and swell waves. As expected, the RMSE and Bias of the three wave periods in high sea states are generally larger than those of low sea states. Comparing the results of Fig. 15 and Table II, it is evident that the estimation of mean wave periods (MWPs) in the two moderate sea states is better than that in the two extreme sea states. This discrepancy is due to the superior energy consistency observed in the omni-directional spectra of the two moderate sea states. The residual trends in mean wave period estimation mirror those of the omnidirectional spectrum estimation in Fig. 15: Shorter MWPs are overestimated but longer MWPs are underestimated. For the sea state of $4.5\,\mathrm{m} \geq H_s > 3\,\mathrm{m}$, Fig. 15(b) illustrates a more favorable fitting for k below approximately

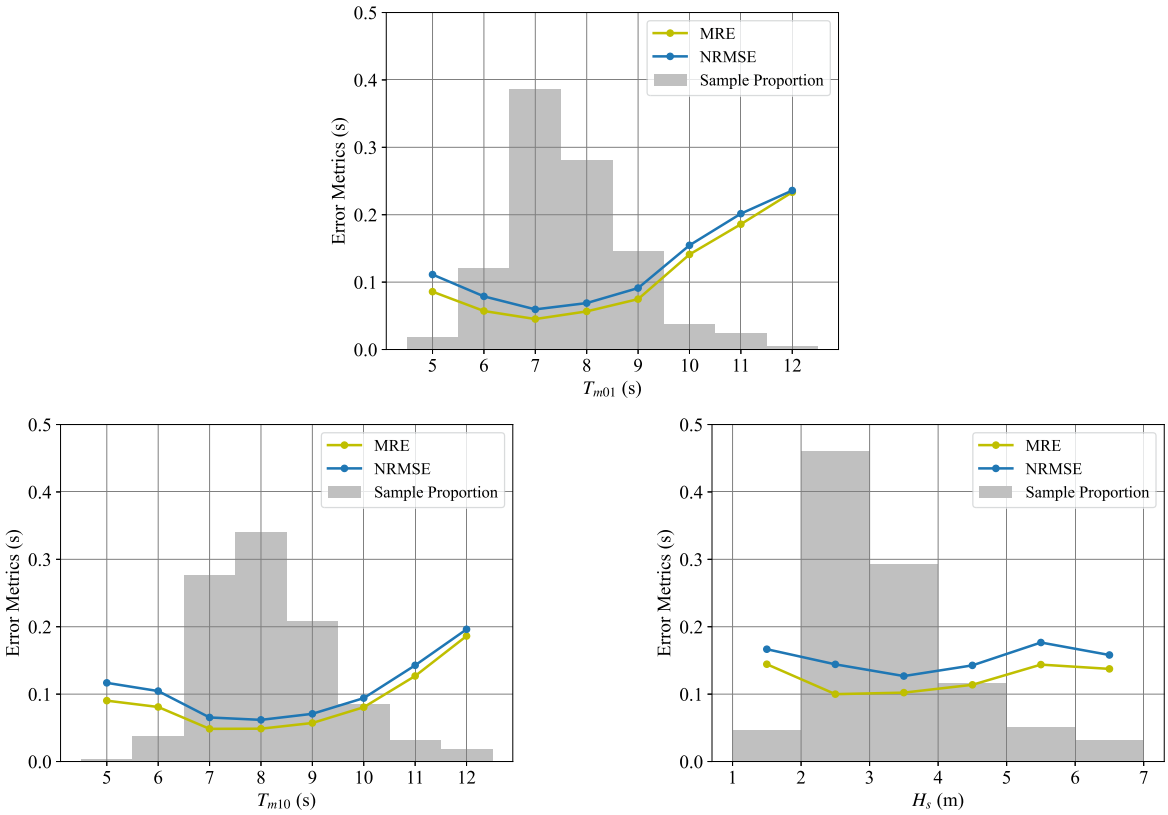

Fig. 17. Comparison of the sample proportion with MRE and NRMSE.

0.01 rd/m compared to k above this value. Therefore, the retrieval performance of T_{m-10} is better than that of T_{m02} in the sea state of $4.5\,\text{m} \geq H_s > 3\,\text{m}$. Fig. 17 further contrasts the sample distribution with Mean Relative Error (MRE) and Normalized RMSE (NRMSE) and reveals a decreasing error trend with an increase in data size for the four parameters calculated from wave spectra.

In the work of Lin et al. [50], they utilized the Parameterized First-guess Spectrum Method (PFSM) to retrieve wave spectra from 50 VV-polarization Sentinel-1 SAR imagettes in IW mode over China's seas. When comparing their retrieval wave spectra with ECMWF reanalysis wave data, the evaluation metrics for T_{m02} exhibited a Bias of –1.11 s, RMSE of 2.43 s, and STD of 2.21 s. In contrary, our T_{m02} yields a Bias of 0.1633 s, and RMSE of 0.6206 s. Johnsen et al. [51] assessed the mean wave period T_{m-10} from the ASAR WM products and the WAM spectra during May, September, and December 2004. Their evaluation showed an RMSE and Bias of 1.3 s and 1.1 s for T_{m-10}, and 0.6 m and –0.2 m for H_s. In comparison, our retrieval method show better results for T_{m-10}, T_{m02}, and significant wave height than those reported by Lin et al. and Johnsen et al. Furthermore, Johnsen et al. also assessed wave direction for retrieval wave spectra from ASAR and reported an RMSE and Bias of approximately 0.9 rd (51.56°) and 0.02 rd (1.146°), respectively. Our wave direction retrieval results exhibit lower RMSE across four sea states, although the Bias, particularly in the lowest sea state, requires improvement.

VI. Conclusion

In this work, we focus on the intricacies of the 2-D wave spectrum retrieval problem using the Gaofen-3 SAR wave mode data and ERA-5 2-D wave spectra. Specifically, we propose a universal two-stage retrieval wave spectrum strategy consisting of energy distribution retrieval and energy intensity retrieval. In the first step, our focus is on retrieving normalized wave spectra using the proposed EA-CGAN. The generator of the EA-CGAN establishes a direct and nonlinear transformation from normalized SAR cross spectra to normalized wave spectra. Benefiting from the imagination capability of EA-CGAN, we achieve the generation of complete 2-D wave spectra from SAR cross-spectra without requiring additional inputs. The second step involves the retrieval of significant wave height (H_s) values from 24 SAR scalar features based on the XGBoost regression model. The combination of normalized wave spectra and obtained significant wave height values results in the ultimate wave spectra. The SAR cross spectra make significant contribution to the shape of retrieval wave spectra and the wave parameters related to the energy density, such as wave period, peak period, and peak direction. The 24 SAR scalar features influence the performance of practical intensity of retrieval wave spectra.

We finally compare our proposed strategy with some of the existing wave spectrum retrieval methods, including MPI, PFSM, and PARSA methods. The key observations are summarized as follows.

1) *MPI, PFSM, and PARSA Methods:* While these methods have shown promising wave spectrum retrieval results over the last a few decades, they are limited by the complex calculation processes associated with nonlinear transformations and the need for prior information as the first guess wave spectra. Our proposed method can effectively reduce the time consumption for wave spectrum retrieval. The generator of the EA-CGAN directly establishes the nonlinear transformation from SAR cross spectra to wave spectra after training, eliminating the need for iterative computations of the loss function. It has been shown that retrieving wave spectra for the total test data (4202) takes only 5 min, with each SAR cross-spectrum requiring only 5 s. Importantly, our method does not need prior information as necessary inputs, which enhances its applicability to other satellites.
2) *Cross Spectrum-Based Wave Retrieval Method:* While this method eliminates the need for an additional spectrum, it is constrained by poor azimuth resolution. Its retrieval performance is compromised due to the presence of a cutoff wavenumber. The azimuth wave information beyond the cutoff wavenumber in the SAR cross-spectrum becomes distorted, which then causes a significant challenge in achieving complete wave spectra retrieval without supplementary wave information inputs. In contrast, in our proposed approach the generator efficiently extracts information from the Gaofen-3 SAR cross-spectrum during the training stage and attempts to generate new information associated with the target ERA-5 wave-spectrum data. After the training, the generator is equipped with the capability to complement specific wave spectrum information based on each SAR cross-spectrum. This dynamic adaptability enhances the robustness of our method, making it adept at addressing the limitations posed by cutoff wavenumbers in cross-spectrum-based wave retrieval methods.
3) *Limitations and Future Work:* Despite the advantages listed above, our method has limitations in the process of removing the 180° ambiguity, particularly when influenced by the positive peak in the imaginary part of the cross-spectrum. The removal performance is constrained when the wave spectrum exhibits multiple peaks in opposite directions. In addition, the H_s retrieval model can be improved, especially in scenarios involving wave breaking, which is a crucial influencing factor for wave characteristics. For this reason, incorporating the steepness variable, which scales the breaking intensity [52], will be part of our future work. Looking forward, we aim to expand our dataset by including buoy data, additional SWIM spectral data, wave model outputs, and altimeter data. This expansion will not only diversify our training set, but also enhance the robustness of our model's validation.

ACKNOWLEDGMENT

The authors would like to thank the Chinese National Satellite Ocean Application Service (NSOAS) for providing the Gaofen-3 SAR wave mode data via https://osdds.nsoas.org.cn/ (registration required), and the ECMWF for providing the ERA5 wave spectra data.

REFERENCES

[1] J. Portilla-Yandún, F. Barbariol, A. Benetazzo, and L. Cavaleri, "On the statistical analysis of ocean wave directional spectra," *Ocean Eng.*, vol. 189, 2019, Art. no. 106361.
[2] K. Hasselmann and S. Hasselmann, "On the nonlinear mapping of an ocean wave spectrum into a synthetic aperture radar image spectrum and its inversion," *J. Geophysical Res.: Oceans*, vol. 96, no. C6, pp. 10713–10729, 1991.
[3] H. E. Krogstad, "A simple derivation of Hasselmann's nonlinear ocean-synthetic aperture radar transform," *J. Geophysical Res.: Oceans*, vol. 97, no. C2, pp. 2421–2425, 1992.
[4] S. Hasselmann, C. Brüning, K. Hasselmann, and P. Heimbach, "An improved algorithm for the retrieval of ocean wave spectra from synthetic aperture radar image spectra," *J. Geophysical Res.: Oceans*, vol. 101, no. C7, pp. 16615–16629, 1996.
[5] G. Engen, H. Johnsen, H. E. Krogstad, and S. F. Barstow, "Directional wave spectra by inversion of ERS-1 synthetic aperture radar ocean imagery," *IEEE Trans. Geosci. Remote Sens.*, vol. 32, no. 2, pp. 340–352, Mar. 1994.
[6] A. Voorrips, C. Mastenbroek, and B. Hansen, "Validation of two algorithms to retrieve ocean wave spectra from ERS synthetic aperture radar," *J. Geophysical Res.: Oceans*, vol. 106, no. C8, pp. 16825–16840, 2001.
[7] X. Li, T. Koenig, J. Schulz-Stellenfleth, and S. Lehner, "Validation and intercomparison of ocean wave spectra inversion schemes using ASAR wave mode data," *Int. J. Remote Sens.*, vol. 31, no. 17-18, pp. 4969–4993, 2010.
[8] W. Shao, X. Jiang, Z. Sun, Y. Hu, A. Marino, and Y. Zhang, "Evaluation of wave retrieval for Chinese Gaofen-3 synthetic aperture radar," *Geo-Spatial Inf. Sci.*, vol. 25, no. 2, pp. 229–243, 2022.
[9] B. Zhang, W. Perrie, and Y. He, "Validation of RADARSAT-2 fully polarimetric SAR measurements of ocean surface waves," *J. Geophysical Res.: Oceans*, vol. 115, no. C6, 2010.
[10] K. Hasselmann et al., "Theory of synthetic aperture radar ocean imaging: A marsen view," *J. Geophysical Res.: Oceans*, vol. 90, no. C3, pp. 4659–4686, 1985.
[11] C. Brüning, S. Hasselmann, K. Hasselmann, S. Lehner, and T. Gerling, "On the extraction of ocean wave spectra from ERS-1 SAR wave mode image spectra," in *1st ERS-1 Symp. Space Serv. our Environ.*, 1993, pp. 747–752.
[12] C. Mastenbroek and C. De Valk, "A semiparametric algorithm to retrieve ocean wave spectra from synthetic aperture radar," *J. Geophysical Res.: Oceans*, vol. 105, no. C2, pp. 3497–3516, 2000.
[13] S. Jian and G. Changlong, "Parameterized first-guess spectrum method for retrieving directional spectrum of swell-dominated waves and huge waves from sar images," *Chin. J. Oceanol. Limnol.*, vol. 24, no. 1, pp. 12–20, 2006.
[14] G. Engen and H. Johnsen, "SAR-ocean wave inversion using image cross spectra," *IEEE Trans. Geosci. Remote Sens.*, vol. 33, no. 4, pp. 1047–1056, Jul. 1995.
[15] H. Johnsen, G. Engen, B. Chapron, N. Walker, and Y. Desnos, "The ASAR wave mode: Level 1 and 2 algorithms and products," in *Proc. ENVISAT Calibration Rev.*, Nordwijk, Netherlands, 2002.
[16] J. Schulz-Stellenfleth, S. Lehner, and D. Hoja, "A parametric scheme for the retrieval of two-dimensional ocean wave spectra from synthetic aperture radar look cross spectra," *J. Geophysical Res.: Oceans*, vol. 110, no. C05004, 2005, doi: 10.1029/2004JC002822.
[17] R. Romeiser, A. Schmidt, and W. Alpers, "A three-scale composite surface model for the ocean wave–radar modulation transfer function," *J. Geophysical Res.: Oceans*, vol. 99, no. C5, pp. 9785–9801, 1994.
[18] J. Schulz-Stellenfleth, T. König, and S. Lehner, "An empirical approach for the retrieval of integral ocean wave parameters from synthetic aperture radar data," *J. Geophysical Res.: Oceans*, vol. 112, no. C03019, 2007, doi: 10.1029/2006JC003970. [Online]. Available: https://agupubs.onlinelibrary.wiley.com/doi/abs/10.1029/2006JC003970
[19] X.-M. Li, S. Lehner, and T. Bruns, "Ocean wave integral parameter measurements using envisat ASAR wave mode data," *IEEE Trans. Geosci. Remote Sens.*, vol. 49, no. 1, pp. 155–174, Jan. 2011.
[20] J. E. Stopa and A. Mouche, "Significant wave heights from Sentinel-1 SAR: Validation and applications," *J. Geophysical Res.: Oceans*, vol. 122, no. 3, pp. 1827–1848, 2017.

[21] H. Wang, J. Zhu, J. Yang, and C. Shi, "A semiempirical algorithm for SAR wave height retrieval and its validation using envisat ASAR wave mode data," *Acta Oceanologica Sinica*, vol. 31, pp. 59–66, 2012.
[22] L. Ren, J. Yang, G. Zheng, and J. Wang, "Significant wave height estimation using azimuth cutoff of C-band RADARSAT-2 single-polarization SAR images," *Acta Oceanologica Sinica*, vol. 34, pp. 93–101, 2015.
[23] G. Grieco, W. Lin, M. Migliaccio, F. Nirchio, and M. Portabella, "Dependency of the Sentinel-1 azimuth wavelength cut-off on significant wave height and wind speed," *Int. J. Remote Sens.*, vol. 37, no. 21, pp. 5086–5104, 2016.
[24] H. Wang et al., "Empirical algorithm for significant wave height retrieval from wave mode data provided by the chinese satellite Gaofen-3," *Remote Sens.*, vol. 10, no. 3, 2018, Art. no. 363.
[25] F. S. Pramudya, J. Pan, A. T. Devlin, and H. Lin, "Enhanced estimation of significant wave height with dual-polarization sentinel-1 SAR imagery," *Remote Sens.*, vol. 13, no. 1, 2021, Art. no. 124.
[26] L. Bao et al., "Impact of polarization basis on wind and wave parameters estimation using the azimuth cutoff from GF-3 SAR imagery," *IEEE Trans. Geosci. Remote Sens.*, vol. 60, 2022, Art. no. 5234716.
[27] C. Fan, T. Song, Q. Yan, J. Meng, Y. Wu, and J. Zhang, "Evaluation of multi-incidence angle polarimetric Gaofen-3 SAR wave mode data for significant wave height retrieval," *Remote Sens.*, vol. 14, no. 21, 2022, Art. no. 5480.
[28] M. J. Collins, M. Ma, and M. Dabboor, "On the effect of polarization and incidence angle on the estimation of significant wave height from SAR data," *IEEE Trans. Geosci. Remote Sens.*, vol. 57, no. 7, pp. 4529–4543, Jul. 2019.
[29] W. Shao et al., "Wave retrieval under typhoon conditions using a machine learning method applied to Gaofen-3 SAR imagery," *Can. J. Remote Sens.*, vol. 45, no. 6, pp. 723–732, 2019.
[30] T. Song, Q. Yan, C. Fan, J. Meng, Y. Wu, and J. Zhang, "Significant wave height retrieval using xgboost from polarimetric Gaofen-3 SAR and feature importance analysis," *Remote Sens.*, vol. 15, no. 1, 2022, Art. no. 149.
[31] B. Quach, Y. Glaser, J. E. Stopa, A. A. Mouche, and P. Sadowski, "Deep learning for predicting significant wave height from synthetic aperture radar," *IEEE Trans. Geosci. Remote Sens.*, vol. 59, no. 3, pp. 1859–1867, Mar. 2021.
[32] H. Wang et al., "Quad-polarimetric sar sea state retrieval algorithm from Chinese Gaofen-3 wave mode imagettes via deep learning," *Remote Sens. Environ.*, vol. 273, 2022, Art. no. 112969.
[33] I. Goodfellow et al., "Generative adversarial nets," in *Proc. Int. Conf. Neural Inf. Process. Syst.*, 2014, pp. 2672–2680.
[34] X. Tai, M. Li, M. Xiang, and P. Ren, "A mutual guide framework for training hyperspectral image classifiers with small data," *IEEE Trans. Geosci. Remote Sens.*, vol. 60, 2021, Art. no. 5510417.
[35] Q. Yang, Z. Ni, and P. Ren, "Meta captioning: A meta learning based remote sensing image captioning framework," *ISPRS J. Photogrammetry Remote Sens.*, vol. 186, pp. 190–200, 2022.
[36] J. Schulz-Stellenfleth and S. Lehner, "Measurement of 2-D sea surface elevation fields using complex synthetic aperture radar data," *IEEE Trans. Geosci. Remote Sens.*, vol. 42, no. 6, pp. 1149–1160, Jun. 2004.
[37] H. Hersbach et al., "The era5 global reanalysis," *Quart. J. Roy. Meteorological Soc.*, vol. 146, no. 730, pp. 1999–2049, 2020.
[38] J. Verron et al., "The saral/altika altimetry satellite mission," *Mar. Geodesy*, vol. 38, no. sup1, pp. 2–21, 2015.
[39] M. Kwant, "Remote sensing of swell waves in the north sea with Sentinel-1 synthetic aperture radar," Ph.D. thesis, Delft Univ. Technol., 2017.
[40] M. Bao and W. Alpers, "On the cross spectrum between individual-look synthetic aperture radar images of ocean waves," *IEEE Trans. Geosci. Remote Sens.*, vol. 36, no. 3, pp. 922–932, May 1998.
[41] V. Kerbaol, B. Chapron, and P. W. Vachon, "Analysis of ers-1/2 synthetic aperture radar wave mode imagettes," *J. Geophysical Res.: Oceans*, vol. 103, no. C4, pp. 7833–7846, 1998. [Online]. Available: https://agupubs.onlinelibrary.wiley.com/doi/abs/10.1029/97JC01579
[42] H. L. Tolman, "Modeling wind waves using wavenumber-direction spectra and a variable wavenumber grid," *Glob. Atmos. Ocean Syst.*, vol. 6, pp. 295–309, 1998.
[43] G. Dong, W. Huang, W. A. Smith, and P. Ren, "A shadow constrained conditional generative adversarial net for SRTM data restoration," *Remote Sens. Environ.*, vol. 237, 2020, Art. no. 111602.
[44] S. Ioffe and C. Szegedy, "Batch normalization: Accelerating deep network training by reducing internal covariate shift," in *Proc. Int. Conf. Mach. Learn.*, 2015, Art. no. 5808102. [Online]. Available: https://api.semanticscholar.org/CorpusID
[45] O. Ronneberger, P. Fischer, and T. Brox, "U-Net: Convolutional networks for biomedical image segmentation," in *Proc. 18th Int. Conf., Med. Image Comput. Computer-Assist. Interv.* 2015, Munich, Germany, pp. 234–241.
[46] A. Zhu, Y. Meng, and C. Zhang, "An improved Adam algorithm using look-ahead," in *Proc. Int. Conf. Deep Learn. Technol.*, 2017, pp. 19–22.
[47] L. Yue, H. Shen, J. Li, Q. Yuan, H. Zhang, and L. Zhang, "Image super-resolution: The techniques, applications, and future," *Signal Process.*, vol. 128, pp. 389–408, 2016.
[48] Y. Xu et al., "Statistical comparison of ocean wave directional spectra derived from SWIM/CFOSAT satellite observations and from buoy observations," *IEEE Trans. Geosci. Remote Sens.*, vol. 60, 2022, Art. no. 5117520.
[49] E. Mackay, C. Retzler, P. Challenor, and C. Gommenginger, "A parametric model for ocean wave period from k_u band altimeter data," *J. Geophysical Res.: Oceans*, vol. 113, no. C03029, 2008.
[50] B. Lin et al., "Development and validation of an ocean wave retrieval algorithm for vv-polarization Sentinel-1 SAR data," *Acta Oceanologica Sinica*, vol. 36, pp. 95–101, 2017.
[51] H. Johnsen, G. Engen, F. Collard, V. Kerbaol, and B. Chapron, "Envisat ASAR wave mode products-quality assessment and algorithm upgrade," in *Proc. SEASAR Eur. Space Agency Spec. Publ.*, 2006.
[52] R. Cao, E. Padilla, and A. Callaghan, "The influence of bandwidth on the energetics of intermediate to deep water laboratory breaking waves," *J. Fluid Mechanics*, vol. 971, 2023, Art. no. A11.

Yuxin Fang received the B.Eng. degree in electronic and information engineering from the China University of Petroleum (East China), Qingdao, China. He is currently working toward the Ph.D. degree in marine resources information engineering with the China University of Petroleum (East China), Qingdao, China.

He is currently a Visiting Ph.D. Student with the Imperial College London, London, U.K. His current research interests include machine learning and deep learning, with applications to remote sensing.

Chenqing Fan received the M.S. degree in electronic and information engineering from the China University of Petroleum, Qingdao, China, in 2009.

He is currently an Associate Researcher with the First Institute of Oceanography, Ministry of Natural Resources, Qingdao. His research interests include radar altimeter, microwave radar imaging, and ocean remote sensing.

Rui Cao received the M.Sc. degree in engineering fluid mechanics, in 2018, from Imperial College London, London, U.K., where he is currently working toward the Ph.D. degree in fluid mechanics by the support of a Skempton Scholarship.

His research interests include fluid mechanics within the two-phase flow by wave breaking, air–wave interactions, and the application of techniques related to remote sensing, image processing, and machine learning on oceanography.

Junmin Meng received the Ph.D. degree in physical oceanography from the Ocean University of China, Qingdao, China, in 2002.

In 2002, he joined the First Institute of Oceanography, State Oceanic Administration (SOA) (Ministry of Natural Resources of the People's Republic of China (MNR) now), Beijing, China. From 2004 to 2009, he was an Associate Research Professor. Since 2009, he has been a Research Professor. His research interests include ocean internal wave and synthetic aperture radar (SAR) marine applications.

Jie Zhang received the Ph.D. degree in applied mathematics from Tsinghua University, Beijing, China, in 1993.

He is currently a Professor with the First Institute of Oceanography, Ministry of Natural Resources, and also the Dean of the College of Oceanography and Space Informatics, China University of Petroleum (East China), Qingdao, China. His research interests include remote sensing and oceanography.

Qiushuang Yan received the Ph.D. degree in ocean exploration technology from the Ocean University of China, Qingdao, China, in 2018.

She is currently working with the School of Oceanography and Spatial Information, China University of Petroleum (East China), Dongying, China. Her research interests include the mechanism of microwave remote sensing in the ocean and the detection methods of wind and wave currents.